Chelate Complexes of 3d Transition Metal Ions – A Challenge for Electronic-Structure Methods?

Lukas Hehn[1], Peter Deglmann[2], and Michael Kühn[1]*

[1] *BASF SE, Next Generation Computing, Pfalzgrafenstr. 1, 67061 Ludwigshafen, Germany*
[2] *BASF SE, Quantum Chemistry, Carl-Bosch-Str. 38, 67063 Ludwigshafen, Germany*

(Dated: December 6, 2023)

Different electronic-structure methods were assessed for their ability to predict two important properties of the industrially relevant chelating agent nitrilotriacetic acid (NTA): its selectivity with respect to six different first-row transition metal ions and the spin-state energetics of its complex with Fe(III). The investigated methods encompassed density functional theory (DFT), the random phase approximation (RPA), coupled cluster (CC) theory, the auxiliary-field quantum Monte-Carlo (AFQMC) method, as well as the complete active space self-consistent field (CASSCF) method and the respective on-top methods second-order N-electron valence state perturbation theory (NEVPT2) and multiconfiguration pair-density functional theory (MC-PDFT). Different strategies for selecting active spaces were explored and the density matrix renormalization group (DMRG) approach was used to solve the largest active spaces. Despite somewhat ambiguous multi-reference diagnostics, most methods gave relatively good agreement with experimental data for the chemical reactions connected to the selectivity, which only involved transition-metal complexes in their high-spin state. CC methods yielded the highest accuracy followed by range-separated DFT and AFQMC. We discussed in detail that even higher accuracies can be obtained with NEVPT2, under the prerequisite that consistent active spaces along the entire chemical reaction can be selected, which was not the case for reactions involving Fe(III). A bigger challenge for electronic-structure methods was the prediction of the spin-state energetics, which additionally involved lower spin states that exhibited larger multi-reference diagnostics. Conceptually different, typically accurate methods ranging from CC theory via DMRG-NEVPT2 in combination with large active spaces to AFQMC agreed well that the high-spin state is energetically significantly favored over the other spin states. This was in contrast to most DFT functionals and RPA which yielded a smaller stabilization and some common DFT functionals and MC-PDFT even predicting the low-spin state to be energetically most favorable.

I. INTRODUCTION

Transition metals (TMs) are key components of many important industrially relevant materials such as catalysts [1–3] and battery materials [4–6] as well as biological systems. [7–10] In an industrial context, quantum-chemical simulations by means of electronic-structure methods have become an integral part in the development of such materials as they, in principle, allow for an enhanced effectiveness and efficiency of corresponding research activities, due to an improved microscopic understanding as well as a potential reduction of the number of time-consuming and expensive lab and production trials. However, a prerequisite for this is that the applied electronic-structure methods allow for sufficiently accurate predictions, while at the same time being computationally efficient.

To that end, many works exist in the literature that individually benchmark the performance of density functional theory (DFT) utilizing a large variety of different density functionals [11–23], the random phase approximation (RPA) [24–26] as well as single-reference wavefunction-based methods such as coupled cluster (CC) theory [27–29] including efficient local CC methods, [30] and Møller-Plesset (MP) perturbation theory [28, 31] for the simulation of TM compounds.

TM compounds are often mentioned as one of the prime examples for multi-reference (or strongly correlated) systems, but at the same time, do not necessarily exhibit multi-reference character in all cases. [32–35] In general, true multi-reference systems are known to not be adequately treatable by the aforementioned single-reference methods. To this end, for the simulation of multi-reference TM systems, active space methods such as the complete active space self-consistent field (CASSCF) method, usually combined with on-top methods like complete active space second-order perturbation theory (CASPT2), [36–38] second-order N-electron valence state perturbation theory (NEVPT2), [39–41] and multiconfiguration pair-density functional theory (MC-PDFT), [42, 43] are a natural choice and thus have been benchmarked extensively as well. The density matrix renormalization group (DMRG) approach is an efficient matrix product state technique that can be combined with the above-mentioned approaches to allow for simulations of larger active spaces and thus has also been applied in the context of TM systems, although to a lesser extend than most of the other methods mentioned above. [44–46] Furthermore, auxiliary-field quantum Monte-Carlo (AFQMC) is a promising method for the simulation of multi-reference systems as well, which

* Corresponding author: michael.b.kuehn@basf.com

does not necessarily rely on a – oftentimes challenging – selection of an active space. However, only rather few works exist on chemical applications of this method. [47–49]

So far, no consensus could be found with respect to which electronic-structure method consistently yields the highest accuracy for a broad variety of compounds, and methods that work well for one or more classes of compounds and a certain target quantity to be calculated are often found to be outperformed by different methods in the context of different applications. For instance, Maurer *et al.* [11] found that the performance of density functionals is in agreement with Jacob's ladder, while Determan *et al.* [12] observed that non-hybrid density functionals can arrive at accuracies comparable to or better than those obtained with hybrid functionals, both working with large sets of 3d TM compounds. Coupled cluster singles and doubles with a perturbative treatment of the triples excitations (CCSD(T)) is often considered the "gold standard" method in quantum chemistry, and is used in Refs. [11, 13] as a reference to assess the accuracy of DFT for a wide range of TM compounds. Indeed, it even performs very well compared to CASPT2 and NEVPT2 as shown in the works of Radoń *et al.* [50–52] However, Xu *et al.* found that CCSD(T) and even higher-order CC methods are not in general better than DFT and cannot simply be used as a reference for theory benchmarks on TM systems. [53]

While most of these studies focus on benchmarking the performance of a few electronic-structure methods on a relatively large set of molecular compounds, the goal of our work is to examine the performance of a larger variety of different methods on a smaller set of properties and chemical reactions of industrially highly relevant chelate complexes of 3d TMs, for which experimental data is available and used as a reference. [54] The methods we study encompass DFT using different density functionals, including the deep neural network parameterized DeepMind 21 (DM21) functional, [55] RPA, [56–58] second-order Møller-Plesset perturbation theory (MP2), [59] CCSD(T), [60, 61] both with and without the domain-based local pair natural orbitals (DLPNO) approximation, [62, 63] and AFQMC in combination with Hartree-Fock and a CASSCF trial wavefunction. [64] Furthermore, we employ CASSCF, [65, 66] combined with the on-top methods NEVPT2 [67] and MC-PDFT, [68–71] and use DMRG in the form of DMRG-CASSCF [72, 73] and DMRG-NEVPT2, [74] enabling the calculation of larger active spaces. Within the active space methods, we also study different strategies for constructing an AS, such as the unrestricted natural orbitals (UNOs) approach, [75] the atomic valence active space (AVAS) method, [76] and using single-orbital entropies as a selection criterion. [77]

The materials of interest for our study are chelating agents and their interaction with 3d TM ions. Chelating agents represent a technically highly relevant class of substances, many of which are industrially produced at large scale. [78–83] Among many others, major areas of use comprise water softeners in cleaning applications, modulators of redox behavior for TMs in oxidative bleaching, scale suppressants, soil remediation and ligands for catalysts. In most applications, the mode of action of chelating agents is to bind several electron donating atoms (lone pairs of electrons) to one typically more than singly positively charged metal center, in particular a TM center. This is reflected in their name, derived from the old Greek word for crab pincers. Thus, chelating agents represent multidentate organic ligands, where the donor centers are typically either neutral or singly negatively charged.

The particularly strong binding of chelating agents to metal cations (chelate effect) can be explained with the negative enthalpy of each donor-metal interaction which sums up almost linearly with the number of these interactions, whereas the entropic penalty for all these interactions is not much higher than the entropy for letting a monodentate ligand (e.g. water) interact with the metal cation. Many technically important chelating agents contain more than two donor atoms, reflecting the fact that the metals relevant to many applications named before prefer coordination via four to eight donors. As a neutral donor atom, nitrogen (as amine, sometimes also imine) is the most prominent choice from a technical perspective, although oxygen (as ether or alcohol), sulfur (as thioether or thiol) and phosphorous (as phosphine or phosphite) also play important roles in specific applications. Among anionic donor functionalities, carboxylates (monoanionic) and phosphonates (dianionic) account for the largest-scale applications.

In many of the aforementioned uses, the interaction of chelating agents with TM centers is key to the desired application property. Thus a reliable computational protocol that yields an accurate and balanced (with respect to coordination modes and spin state) description of such systems would be highly desirable from an industrial perspective. To enable a broad comparison of electronic-structure methods in this benchmark study, as an exemplary ligand, the relatively small aminocarboxylate nitrilotriacetic acid was selected. [84–87] It represents a trianionic ligand with one amino and three carboxylate donors and is thus chemistry-wise rather representative. It furthermore offers the advantage that there are not too many different conformations possible – in contrast to some other important aminocarboxylates or phosphonates. Finally, its complexes with dicationic and tricationic metal ions are either neutral or singly negatively charged, so that there are good reasons to assume that solvation treatment – although it will definitely matter – will hopefully not overrule all the other aspects considered in this study and the error with respect to experimental data is mostly due to the error in the single-point energy obtained with the electronic-structure method. As an example system, the structure of the neutral Fe(III)-NTA complex [FeNTA(H_2O)$_2$] is shown in Figure 1, wherein NTA in the following de-

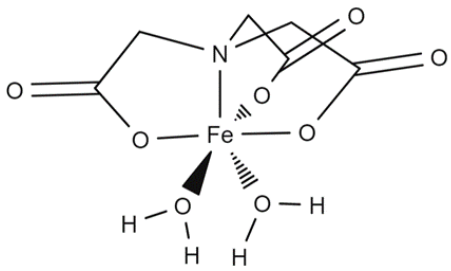

FIG. 1. Structural formula of the Fe(III)-NTA complex $[FeNTA(H_2O)_2]$.

notes the trianion obtained by deprotonating nitrilotriacetic acid, which forms a coordination complex with the metal ion.

The property that this work focuses on is the selectivity of the NTA chelating agent with respect to various 3d TM ions in aqueous solution. Put simply, the selectivity describes how strongly a chelating agent prefers to bind to a specific metal ion over another metal ion, and is thus an important industrially relevant application property. The selectivity is determined via calculation of the Gibbs free energy of the following chemical reaction in aqueous solution at standard ambient conditions, $\Delta_r G^0$:

$$[M_1\,\mathrm{NTA}\,(\mathrm{H_2O})_x]^{n_1-3} + [M_2\,(\mathrm{H_2O})_6]^{n_2+} \rightleftharpoons [M_2\,\mathrm{NTA}\,(\mathrm{H_2O})_y]^{n_2-3} + [M_1\,(\mathrm{H_2O})_6]^{n_1+} + (x-y)\,\mathrm{H_2O}\ . \quad (1)$$

M_1 and M_2 are the two metal ions with their respective charges n_1 and n_2. The final H_2O term accounts for different amounts of water molecules explicitly coordinating to the metal center. The different first-row TM ions M studied in this work are: Fe(III), Mn(II), Fe(II), Co(II), Ni(II), and Cu(II).

One of the prerequisites for the calculation of the selectivity is the understanding of the spin-state energetics of each individual compound involved in Equation 1. In particular, the energetically most favorable electron configuration of each compound has to be determined, which is not only influenced by the electron configuration of the 3d orbitals at the TM center, but also by their interaction with the NTA ligand. While the spin-state energetics of some aqua complexes have been studied in detail, [50, 51] to the best of our knowledge, comparable investigations for TM complexes of the chemically rather representative chelating agent NTA are nonexistent. Therefore, another focus of this work is on the calculation of the spin-state energetics, i.e. the relative energies of the high-spin, intermediate-spin and low-spin state of the Fe(III)-NTA complex shown in Figure 1 using the methods mentioned above. The results of this analysis are then used to decide on the energetically most favorable electron configurations, i.e. spin states, of the TM-NTA complexes relevant for the calculation of the selectivity.

The paper is structured as follows. In section II, details on the electronic-structure methods, corresponding programs and settings are given, as well as on the remainder of the workflow used. In section III A, we present and discuss the performance of those methods with respect to the spin-state energetics of the Fe(III)-NTA complex. In section III B, the results obtained with the those methods for the selectivity of NTA with respect to six different first-row TM ions are presented and compared against experimental data.

II. COMPUTATIONAL DETAILS

A. Structure Optimization and Models

All structures were optimized using the generalized gradient approximation (GGA) functional of Becke and Perdew (BP86) [88] within a spin-unrestricted formalism in combination with Grimme's D3 dispersion correction, [89, 90] and the damping term of Becke and Johnson (D3(BJ)). [91–93] Basis sets of quadruple-ζ valence quality with one set of polarization functions (def2-QZVP) were used. [94, 95] The resolution-of-the-identity (RI) approximation was employed along with suitable auxiliary basis sets. [96] Solvation effects were accounted for via the conductor-like screening model (COSMO), [97] with $\epsilon = 78$ representing water as solvent. We note that Radoń *et al.* found that solvation effects on the structures of hexaaqua complexes of TMs can be very large, but are approximated well by the COSMO model. [50] The calculations were performed using `TURBOMOLE` version 7.5.2. [98–100] Default convergence criteria and grids of size m3 were employed. All calculations were performed on BASF's supercomputer "Quriosity". [101]

We optimized the structures for all feasible spin states: Fe(III)- and Mn(II)-containing compounds assuming 5, 3 and 1, Fe(II)-containing compounds assuming 4, 2, and 0, Co(II)-containing compounds assuming 3 and 1, Ni(II)-containing compounds assuming 2 and 0, and Cu(II)-containing compounds assuming 1 unpaired electrons. Furthermore, preceding the structural optimizations, we performed an iterative conformer search to determine the energetically most stable conformer for each compound and spin state at the same level of theory. Within these conformer searches, stepwise rotations around single bonds with subsequent geometry relaxations have been performed. With the low conformational flexibility of the compounds studied, we consider it unlikely that the minimum-energy conformers identified by this local optimization approach do not correspond to the global conformational optima. Additionally, vibrational frequencies were calculated numerically, and all confirmed to be real, to avoid arriving at any saddle-point structures.

As a prerequisite, it is furthermore necessary to determine the amounts of water molecules in the first coordination sphere of the TM-NTA complexes, i.e. the

amounts of water molecules that need to be taken into account explicitly in the calculations. While for all investigated TM ions it is well established in the literature that they form octahedral hexaaqua complexes in aqueous solution, [102–105] for TM-NTA complexes the situation is less clear. Assuming that reasonably only one or two water molecules can directly coordinate to the TM ions in TM-NTA complexes, we optimized all respective structures and calculated the Gibbs free energy, $\Delta_r G^0$, for the addition of a second explicit water molecule in aqueous solution, to determine the energetically most stable structures:

$$[M\,\mathrm{NTA}\,\mathrm{H_2O}]^{n-3} + \mathrm{H_2O} \rightleftharpoons [M\,\mathrm{NTA}\,(\mathrm{H_2O})_2]^{n-3} \quad , \tag{2}$$

The nomenclature is analogous to that with respect to Equation 1. The results for this, at the B3LYP/def2-TZVP level, are shown in Table V in the Appendix.

B. Single-Point Energies

1. *Density Functional Theory*

Single-point energies were calculated using the two GGA functionals of Becke and Perdew (BP86) [88] and Perdew, Burke, and Ernzerhof (PBE), [106] as well as three meta-GGA functionals, namely the functional of Tao, Perdew, Staroverov, and Scuseria (TPSS) [107], the restored regularized strongly constrained and appropriately normed (r^2SCAN) functional, [108] and the Minnesota 2006 local functional (M06-L), parameterized especially for TM systems. [18] Additionally, four hybrid-(meta-)GGA functionals were used including the hybrid version of TPSS containing 10% nonlocal exchange (TPSSh), [109] Becke's three-parameter hybrid functional with Lee–Yang–Parr correlation containing 20 % nonlocal exchange (B3LYP), [110] the nonempirical hybrid functional PBE0 containing 25 % nonlocal exchange, [111] and the Minnesota 2006 functional with 54% nonlocal exchange (M06-2X). [112] We also evaluated the performance of the range-separated hybrid functional ωB97M-V, [23] as well as of the rather recent DeepMind 21 (DM21) functional based on a deep neural network which was trained on molecular data and exact conditions for fractional charge and spin. [55]

For the BP86, PBE, TPSS, TPSSh, B3LYP and PBE0 functionals, Grimme's D3 dispersion correction together with the damping term of Becke and Johnson (D3(BJ)) was used, while for the Minnesota functionals M06-L and M06-2X the BJ damping term was neglected. The r^2SCAN functional was evaluated both entirely without any dispersion correction, and with the three corrections (D4 dispersion, tailor-made basis set and geometrical counterpoise corrections) provided by the r^2SCAN-3c functional. [113] The ωB97M-V calculations were performed using a self-consistent treatment of the integrated dispersion correction of Vydrov and Van Voorhis (VV10). [114] For the DM21 functional, we extracted the energy contribution originating from the D3(BJ) correction from the respective B3LYP calculations and added those to the DM21 energies.

Basis sets of quadruple-ζ valence quality with two sets of polarization functions (def2-QZVPP) were used, which are also the default basis sets used in our study unless mentioned otherwise. [94, 95] Furthermore, the RI approximation is employed along with suitable auxiliary basis sets. [96] All single-point DFT calculations were performed in the gas phase using the unrestricted Kohn-Sham formalism. `TURBOMOLE` was used, with the exception of DM21 calculations, which were done using `PySCF` version 2.0.1 [115, 116] and the DM21-`PySCF` interface. [117] Default convergence criteria and grids of size m3 were used, except for DM21, for which the convergence criteria are loosened to 10^{-6} for the energy and 10^{-3} for the gradient of the energy, as suggested by the developers. [117]

For the investigation of the spin-state energetics of Fe(III)-NTA in section III A, we also modified the amount of exact exchange in the three hybrid functionals TPSSh, B3LYP, and PBE0 from 0 to 60% in steps of 5%, similar to what Edler and Stein have done in Ref. [118] for the B3LYP functional. We refer to these modified functionals as *FUNC*(X% HF), where *FUNC* can be one of B3LYP, PBE0 and TPSSh and X is the percentage of exact exchange, i.e. Hartree-Fock (HF) exchange.

2. *Random-Phase Approximation*

Random-phase approximation (RPA) [56–58, 119, 120] calculations with and without the approximate exchange kernel (RPA-AXK), [121] using the TPSS functional to generate the Kohn-Sham reference, were carried out employing `TURBOMOLE` in combination with def2-QZVPP basis sets and corresponding auxiliary basis sets. [122, 123] An increased number of frequency quadrature points of 400, which is recommended for small-gap systems, was used.

3. *Coupled Cluster and Møller-Plesset Perturbation Theory*

Coupled cluster singles and doubles with a perturbative treatment of triples excitations (CCSD(T)) calculations were carried out in combination with def2-TZVP basis sets using `TURBOMOLE`. [60, 61, 95] CCSD(T) calculations with the domain-based local pair natural orbital approximation (DLPNO-CCSD(T)) [62, 63] were carried out using `ORCA` version 5.0.2 [124] in combination with def2-TZVPP and def2-QZVPP basis sets and corresponding auxiliary basis sets. [123, 125, 126] Two-point complete basis set (CBS) extrapolations based on the respective results ((3,4)CBS)) were done as well. This is described in more detail in section A in the Appendix.

The convergence settings of the underlying HF reference calculations were tightened to "VeryTightSCF" and the stricter "TightPNO" setting was enabled for the DLPNO-CCSD(T) calculations as recommended in the `ORCA` manual to minimize the error introduced by the DLPNO approximation. [127]

We performed the CCSD(T) calculations using both restricted open-shell Hartree-Fock (ROHF) and unrestricted Hartree-Fock (UHF) molecular orbitals, the full results of which can be seen in Table VII in the Appendix. As differences are small, the DLPNO-CCSD(T) calculations were only carried out using unrestricted molecular orbitals. We additionally explored employing unrestricted TPSS molecular orbitals in the DLPNO-CCSD(T) calculations. Using molecular orbitals obtained with DFT within CC calculations is not common but has been done previously. [128, 129]

Second-order Møller-Plesset perturbation theory (MP2) [59] calculations were carried out analogously to the CCSD(T) calculations described above, using def2-QZVPP basis sets and molecular orbitals from UHF calculations within `TURBOMOLE`. [130] The spin-component scaling and scaled opposite-spin flavors of MP2 (SCS-MP2 and SOS-MP2, respectively) were also used with the default scaling factors in `TURBOMOLE`. [131]

For all calculations described in this section, the following energetically lowest-lying molecular orbitals were excluded from the correlation treatment: 12 for hexaaqua complexes, 21 for NTA complexes of Fe(III), Mn(II), Fe(II), and Ni(II) and 20 for NTA complexes of Co(II) and Cu(II), that contain one less explicit water molecule, see also Table V in the Appendix, and 1 in case of H_2O.

4. *Auxiliary-Field Quantum Monte Carlo*

Auxiliary-field quantum Monte Carlo (AFQMC) [64] calculations were carried out using `ipie` version 0.6.2 [132] with interface to `PySCF`, employing def2-SVP and def2-TZVP basis sets. [95] We used ROHF trial wavefunctions and additionally, for the spin-state energetics of the Fe(III)-NTA complex, (5,5)CASSCF trial wavefunctions, selecting the molecular orbitals with predominantly TM 3d character into the active space, see also section II B 5. A cutoff of 10^{-5} was employed for the Cholesky decomposition of the two-electron integrals. The imaginary time step was set to 0.005 Ha^{-1} and energy measurements were taken every 0.1 Ha^{-1}. All other settings conform to standard `ipie` settings. The frozen core approximation was used analogously to section II B 3. We used 5000 walkers and ran the calculation for 10000 blocks (7000 blocks in the case of a CASSCF trial wavefunction). For the final statistical evaluation the first 500 blocks were discarded to allow for a warm-up phase. Since we were not able to run calculations using Dunning's correlation-consistent basis sets of valence triple-ζ quality (cc-pVTZ) [133] due to the large computational cost of AFQMC, we carried out two-point CBS extrapolations using the the more economical def2-SVP and def2-TZVP basis sets ((2,3)CBS) as described in further detail in section A in the Appendix.

5. *Multi-Reference Active Space Methods*

Multi-reference active space calculations in the form of complete active space self-consistent field (CASSCF) [65, 66] and complete active space configuration interaction (CASCI) calculations were carried out within `PySCF` using def2-QZVPP basis sets. Active spaces containing 18 molecular orbitals or more were solved using density matrix renormalization group (DMRG) theory within `StackBlock` version 1.5.3. [72, 73, 134–137] The respective methods are denoted as DMRG-CASSCF and DMRG-CASCI.

Furthermore, we employed as on-top methods second-order N-electron valence state perturbation theory (NEVPT2) [67] as well as multi-configuration pair density functional theory (MC-PDFT). [68–71] NEVPT2 calculations were based on the strongly contracted internal contraction scheme and were carried out on top of the respective CASSCF wavefunctions. In the cases of DMRG-CASSCF and DMRG-CASCI, we also applied DMRG in the on-top NEVPT2 step (DMRG-NEVPT2) [74]. All DMRG calculations (DMRG-CASSCF, DRMG-CASCI and DMRG-NEVPT2) were done with a maximum bond dimension (MBD) of 1000, except for the largest active spaces in our study with 49 electrons in 36 orbitals, for which the MBD had to be reduced to 600 in the DMRG-NEVPT2 step. Our MC-PDFT calculations employed the translated (t) and fully-translated (ft) versions of the GGA functional PBE and the hybrid functional PBE0 (tPBE, ftPBE, tPBE0, ftPBE0) and were carried out using the MC-PDFT extension for `PySCF`. In section C in the Appendix we describe how we obtained the energies for reactions containing TM-NTA complexes with different amounts of explicit water molecules on reactant and product side.

There are many different strategies for selecting active spaces for the above-described multi-reference active space methods. [75–77, 138–145] In this study, we use several of these techniques, which will be briefly described in the following. A rather straightforward approach to add orbitals of certain character to the active space, e.g. five orbitals with predominantly TM 3d character, is based on a Mulliken population analysis [146] of ROHF orbitals or unrestricted natural orbitals (UNOs) obtained with HF or MP2, [142, 143] which may be combined with localization schemes such as the Pipek-Mezey localization. [147]

Another approach is the atomic valence active space (AVAS) method, [76] which functions via selecting atomic orbitals from an auxiliary atomic basis set, rotating the reference orbitals (e.g. molecular orbitals from a HF calculation) based on an overlap matrix, and applying an overlap threshold to select orbitals into the active

space. In the original work of Sayfutyarova *et al.* this was done exclusively for reference orbitals from single-reference methods such as HF. We modified this approach to work with reference orbitals from previously obtained CASSCF wavefunctions as well, thus allowing for a stepwise expansion of the active space by means of the AVAS technique. In this work, we exclusively use the atomic natural orbital with relativistic contraction (ANO-RCC) basis sets as the auxiliary atomic basis set within the AVAS technique. [148–150]

Another semiautomatic method used in our study is the selection of active orbitals by means of single-orbital entropies (SOEs), which are obtained by first selecting a set of UNOs based on natural occupation numbers and, in a second step, determining single-orbital entropies by means of a DMRG-CASCI calculation within this selected set of UNOs using a rather small MBD. Finally, those orbitals with single-orbital entropies exceeding a certain threshold are selected into the active space. We apply this method using the `ActiveSpaceFinder` software [151] with the default settings (unrestricted MP2 natural occupation numbers between 0.01 and 1.99, MBD of 250, single-orbital entropy threshold of $-0.1\ln(0.25) \approx 0.14$). It should be noted that a similar approach is also implemented within `AutoCAS` by Stein *et al.* [77, 139, 140]

C. Thermodynamics and Solvation Treatment

Both the investigation of the spin-state energetics and the selectivity require the translation of the energies obtained with the aforementioned methods into Gibbs free energies, ΔG^0 and $\Delta_r G^0$, for the respective spin-state transitions and chemical reactions (Equation 1). Solvation in water was done with the COSMO-RS approach, where the abbreviation "RS" stands for "real solvents", [152–154] using version 2018 of the `COSMOtherm` software, [155, 156] and the fine parametrization based on BP86/def2-TZVPD. [157] We used a temperature of 25°C and assumed infinite dilution. The contribution of the vibrational partition function is included in the calculations of the Gibbs free energy. In case of the selectivity, for each metal pair, we assigned M_1 and M_2 such that the experimental $\Delta_r G^0$ would be positive.

III. RESULTS

A. Spin-State Energetics of the Fe(III)-NTA Complex

We use one exemplary NTA complex, with Fe(III) as the central metal ion and two explicit water molecules, see Table V in the Appendix, to investigate the spin-state energetics by applying all electronic-structure methods described in section II. More specifically, we calculate difference in Gibbs free energies, $\Delta_r G^0$, between the high-spin (HS, sextet, $S = 5/2$, $\langle \hat{S}^2 \rangle_{\text{theo}} = 8.75$), intermediate-spin (IS, quartet, $S = 3/2$, $\langle \hat{S}^2 \rangle_{\text{theo}} = 3.75$) and low-spin (LS, doublet, $S = 1/2$, $\langle \hat{S}^2 \rangle_{\text{theo}} = 0.75$) state at the respectively relaxed structures, i.e. we investigate the adiabatic spin-state energetics, with the goal of determining the energetically most favorable spin state in aqueous solution which is a prerequisite for the calculation of the selectivity in section III B.

Distances [pm]	**HS**	**IS**	**LS**
O(H_2O)-Fe (avg.)	218.5	219.7	203.3
O(NTA)-Fe (avg.)	195.5	194.0	188.4
N-Fe	227.8	201.8	195.1

TABLE I. Interatomic distances between the central Fe atom and the atoms of the first coordination sphere for the relaxed structures of each spin-state of Fe(III)-NTA. We distinguish between the three O atoms of the carboxyl groups and the two O atoms of the water molecules and take the average distance within each set.

Interatomic distances for the relaxed structures of the three spin-states are shown in Table I. The HS state with each of the five Fe 3d orbitals being singly occupied has the largest distance between Fe and the NTA donor atoms. In the IS state, the Fe-$3d_{z^2}$ orbital is unoccupied, and the strongest donor atom, nitrogen, can move closer to the Fe(III) center. Due to the structural trans effect [158], one of the H_2O is pushed further away, slightly increasing the average distance of the two H_2O. The LS state then further depopulates the Fe-$3d_{x^2-y^2}$ orbital, allowing the remaining ligands orthogonal to the Fe-N axis to move in closer to the Fe(III) center as well.

Our study on the adiabatic spin-state energetics of Fe(III)-NTA is somewhat analogous to the investigation of the vertical spin-state energetics of the slightly simpler Fe(III)-hexaaqua complex by Radoń *et al.* [50] However, besides focusing on a different molecule, we also evaluate different electronic-structure methods and active spaces with the final goal of going beyond spin-state energetics and studying chemical reactions.

1. *Multi-Reference Diagnostics*

Multi-reference diagnostics can help to determine whether it is expected that a molecule can be accurately simulated with single-reference methods or if multi-reference methods need to be applied. A selection of diagnostics are calculated for the different spin-states of Fe(III)-NTA. Respective results are shown in Table II. For the IS and LS states, deviations between the expectation value $\langle \hat{S}^2 \rangle$ calculated at UHF level and the respective theoretical value indicate non-negligible spin contamination, which can be a first indication of multi-reference character. While the T1 diagnostics only slightly exceed the empirical threshold of 0.02, [159] which marks the borderline between single- and multi-reference cases, the D1 diagnostics clearly exceed the respective threshold of 0.05, [160] ranging between 0.11 for the HS state and 0.18

Diagnostics	HS	IS	LS
$\langle\hat{S}^2\rangle_{\mathrm{UHF}}$ ($\langle\hat{S}^2\rangle_{\mathrm{theo}}$)	8.76 (8.75)	4.03 (3.75)	1.52 (0.75)
T1	0.021	0.023	0.027
D1	0.114	0.179	0.181
# Determinants	1	12	32

TABLE II. Multi-reference diagnostics for the three spin-states of Fe(III)-NTA. The UHF calculation was done in the def2-QZVPP basis and the T1 and D1 diagnostics were obtained from CCSD/def2-TZVP calculations using ROHF orbitals. The number of Slater determinants with squares of CI coefficients $> 10^{-4}$ within a minimal active space calculation including five Fe(III) 3d orbitals at the (5,5)CASSCF/def2-QZVPP level are also given.

for the IS and LS states. Finally, the number of Slater determinants with squares of CI coefficients $> 10^{-4}$ within a minimal-active-space (5,5)CASSCF (including the five Fe(III) 3d orbitals in the active space) show that while for the HS case only a single determinant is required and the wavefunction is identical to the respective ROHF wavefunction, this number rises to 12 and 32 Slater determinants with CI coefficients above the threshold for the IS and LS state, respectively. The squares of the largest CI coefficients amount to 0.97 for the IS state and 0.87 for the LS state. In summary, these diagnostics indicate that multi-reference methods should be considered in particular in case of the IS and LS states, as all diagnostics indicate an increase in multi-reference character with decreasing spin multiplicity.

2. *Density Functional Theory*

The indications of the multi-reference diagnostics, that the calculation of the spin-state energetics of Fe(III)-NTA may be challenging, at least for certain classes of electronic-structure methods, are confirmed by the performance of various density functionals, shown in Figure 2. The Gibbs free energies, ΔG^0, between the different spin states strongly vary between the different functionals within a range of 106 kJ/mol (minimum value: TPSS – maximum value: M06-2X) for the energy gap between IS and HS and even within 216 kJ/mol (DM21 – M06-2X) for the energy gap between LS and HS. When neglecting the results of DM21, which is a rather recent not yet well benchmarked functional, and M06-2X, which is not recommended for TM compounds due to its large amount of HF exchange, the ranges are still within 78 kJ/mol (TPSS – M06-L) for the IS-HS energy gap and 115 kJ/mol (TPSS – M06-L) Most severely, the (meta-)GGA functionals TPSS, BP86 and PBE as well as the DM21 functional favor the LS state instead of the HS state, as opposed to all other functionals and electronic-structure methods except for non-hybrid MC-PDFT, which will be discussed in section III A 3 and section III A 4. While PBE and BP86 only yield a $\Delta_r G^0$ of between −1 to −2 kJ/mol, essentially predicting both

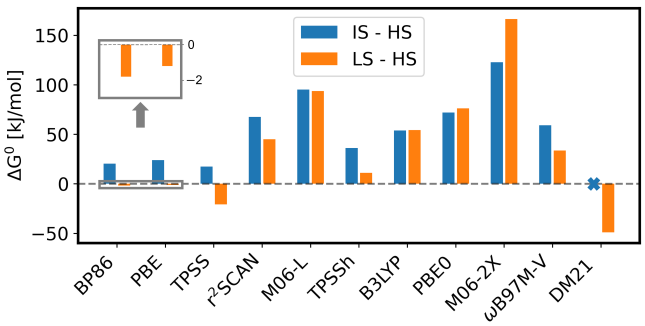

FIG. 2. Spin-state energetics of Fe(III)-NTA using different DFT functionals in combination with def2-QZVPP basis sets. The differences in Gibbs free energies, ΔG^0, between the IS and HS as well as the LS and HS states are plotted. For DM21 we were not able to converge the IS calculation.

HS and LS state to be equal in energy within chemical accuracy, TPSS (−21 kJ/mol) and DM21 (−49 kJ/mol) significantly favor the LS state. The dispersion correction does not have a strong impact on these results, as for example, the B3LYP functional with and without dispersion correction (D3(BJ)) as well as the 3c correction for the r^{2}SCAN functional yield $\Delta_r G^0$ values that differ by less than 5 kJ/mol for both the IS-HS and LS-HS energy gaps. It is noted that, out of all studied functionals, the results obtained with M06-L, which is specifically designed for the simulation of TM compounds, [18] are close to the results of higher-level methods as will be described in section III A 3 and section III A 4.

One particularly notable effect, visible in Figure 2, is that the amount of HF exchange in the density functionals strongly impacts the energy gap between the different spin states, with the HS state being more favored the more HF exchange is present. This can be seen more explicitly in Figure 3, where the LS-HS energy gap is plotted against the amount of HF exchange (X% HF) in the three modified hybrid functionals TPSSh(X% HF), B3LYP(X% HF) and PBE0(X% HF), wherein for TPSSh(10% HF), B3LYP(20% HF) and PBE0(25% HF) the results of the respective unmodified hybrid functionals are recovered, and for TPSSh(0% HF) and PBE0(0% HF) the TPSS and PBE results are obtained, respectively. The analogous plot for the IS-HS energy gap can be found in Figure 19 in the Appendix, showing qualitatively similar behavior. The spin contamination of the functionals is also dependent on the HF exchange, which we show in Figure 17 in the Appendix. The exact slope of the lines in Figure 3 depends on the remainder of the functional, e.g. for TPSSh(X% HF) and PBE0(X% HF) the LS-HS energy gap increases by approximately 3 kJ/mol per % HF exchange while for B3LYP(X% HF) a steeper increase of around 5 kJ/mol per % HF exchange is observed. The LS state is typically favored for amounts of HF exchange of below 10%. While this shouldn't be taken too far, as the functionals are parameterized for the amount of HF exchange they have in

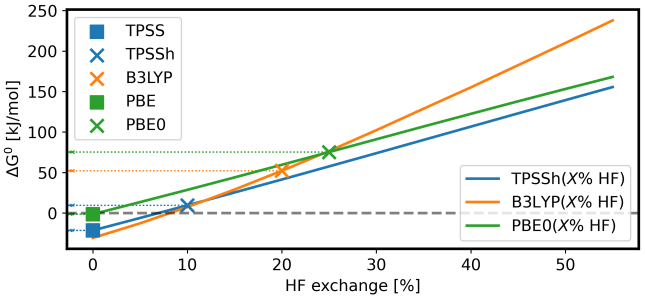

FIG. 3. Influence of the amount of HF exchange in DFT on the energy gap, ΔG^0, between the LS and HS states of Fe(III)-NTA. The amount of HF exchange in the hybrid functionals TPSSh, B3LYP and PBE0 was varied between 0 and 55% in steps of 5%. The points that correspond to the unmodified hybrid functionals as well as their non-hybrid counterparts TPSS and PBE are marked. The basis sets used are def2-QZVPP.

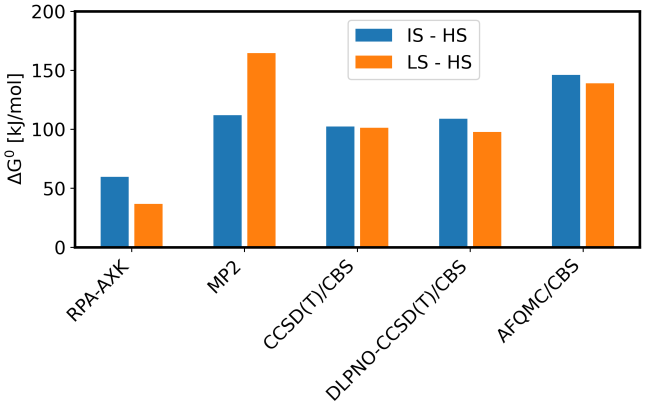

FIG. 4. Spin-state energetics of Fe(III)-NTA using different correlated methods without active spaces. The basis sets used are def2-QZVPP, unless labeled CBS. As the statistical error of the AFQMC results is below 2 kJ/mol, error bars are neglected in the plot. For further information see Figure 2.

their respective unmodified versions, this general trend also matches up with the results of the M06-2X functional, which with its 56% HF exchange clearly favors the HS state by 167 kJ/mol over the LS state. Even the extreme scenario of 100% HF exchange, i.e. a UHF calculation, fits into this trend, where the $\Delta_r G^0$ amounts to 378 kJ/mol for the LS-HS energy gap. Edler and Stein note a similarly strong relationship between the amounts of HF exchange in density functionals and the spin-state energetics of an Fe(III) cluster, also finding a near linear relationship that favors the HS state the more HF exchange is included. [118] Additionally, our findings are also in agreement with the observations by Radoń *et al.* that the (meta-)GGA functionals TPSS and BP86 show significantly smaller energy gaps between different spin states of Fe(III)-hexaaqua than hybrid functionals. [50] This in practice means that one might construct almost any energy gap between the spin states depending on the amount of HF exchange in the selected density functional, making DFT rather unreliable for this purpose.

3. *Correlated Methods Without Active Spaces*

As emphasized before, an at least qualitatively correct prediction of the energetically most favorable spin state is a prerequisite for the calculation of the selectivity in section III B, as well as all other chemical reactions the respective molecule is involved in. Due to the aforementioned shortcomings of DFT, we consult computationally more expensive electronic-structure methods and compare the respective results. In contrast to DFT, all other methods that will be discussed in this section and section III A 4 – with the exception of MC-DFT, which also relies on a density functional – agree that the HS state is energetically clearly favored over the LS and IS states.

The results obtained with correlated methods that do not rely on the selection of active spaces are shown in Figure 4. The main outlier within this group is RPA-AXK, which, possibly due to being based on a TPSS reference, estimates the energy gaps to be 37 kJ/mol (LS-HS) and 60 kJ/mol (IS-HS). Without the AXK correction, RPA predicts even smaller energy gaps of 17 kJ/mol (LS-HS) and 48 kJ/mol (IS-HS). The values obtained with RPA(-AXK) are significantly smaller than the respective energy gaps obtained with CCSD(T) and DLPNO-CCSD(T), which fall between 98 and 109 kJ/mol. The energy gaps obtained with AFQMC are larger, amounting to 139 kJ/mol (LS-HS) and 146 kJ/mol (IS-HS). However, it is noted that, in contrast to DLPNO-CCSD(T) where we could afford the (3,4)CBS extrapolation, we had to rely on the less accurate (2,3)CBS extrapolation in case of AFQMC. For both CCSD(T) and AFQMC, the energy of the LS state is only slightly below the energy of the IS state (within 10 kJ/mol).

For AFQMC we also used a (5,5)CASSCF trial wavefunction in combination with the def2-TZVP basis set. This slightly changes the results compared to AFQMC with a ROHF trial wavefunction shown in Figure 4, reducing the IS-HS energy gap by 3 kJ/mol and the LS-HS energy gap by 7 kJ/mol, bringing it more in line with the DLPNO-CCSD(T)/CBS results, see section E in the Appendix. The statistical error of AFQMC was always below 2 kJ/mol. Due to the large computational cost of AFQMC when using multi-determinant trial wavefunctions, further increasing the size of the active space for the CASSCF trial wavefunction was not feasible.

Within CCSD(T) theory, whether UHF or ROHF molecular orbitals are used changes the final result in the def2-TZVP basis set by at most 3 kJ/mol, see section E in the Appendix. We therefore restrict our discussion to the results obtained when using ROHF molecular orbitals. It is noted that, for MP2, switching from UHF to ROHF molecular orbitals the results change more significantly from 112 to 122 kJ/mol for the IS-HS gap and

from 165 to 111 kJ/mol for the LS-HS gap, bringing them in between the respective CCSD(T) and AFMQC values. For DLPNO-CCSD(T) we were able to perform a (3,4)CBS extrapolation while for CCSD(T) we performed a (2,3)CBS extrapolation. The CBS extrapolation changes the ΔG^0 compared to the largest basis set involved in the extrapolation by at most 8 kJ/mol. To estimate the DLPNO error, we compare DLPNO-CCSD(T) and CCSD(T) in the def2-TZVP basis set, where the error introduced due to the DLPNO approximation is quite high in this case, amounting to 20 kJ/mol (IS-HS) and 27 kJ/mol (LS-HS), although we have applied the "VeryTightSCF" and "TightPNO" settings in `ORCA`, see section II and section E in the Appendix. The respective increase in ΔG^0 due to the DLPNO error is then counterbalanced by a decrease in ΔG^0 when increasing the basis set size to def2-QZVPP or applying the (3,4)CBS extrapolation. Therefore, the rather good agreement of DLPNO-CCSD(T)/(3,4)CBS with CCSD(T)/(2,3)CBS in Figure 4 is at least partly due to the presumably larger (2,3)CBS extrapolation error in case of CCSD(T) being compensated by the DLPNO approximation error in combination with a presumably smaller (3,4)CBS extrapolation error in case of DLPNO-CCSD(T).

4. *Multi-Reference Active Space Methods*

In the following, we discuss the results obtained with multi-reference methods that rely on the selection of active spaces. For selecting the active spaces, we mainly used a Mulliken population analysis of the UNOs obtained with HF. The following active spaces were considered: (5,5) including five 3d orbitals of Fe, (9,12) additionally including five 4d and two σ-bonding orbitals to the ligand by means of the 3d character which is roughly around 10% (analogously to the (9,12) active spaces used by Radoń *et al.* for the Fe(III)-hexaaqua complex [50]), (17,20) additionally including one 3s, three 3p, one 4s and three 4p orbitals as well as (49,36) that furthermore include three 2p orbitals of each ligand atom in the first coordination sphere. Note that for the (49,36) active spaces two such ligand orbitals are already contained in the (17,20) active space as σ-bonding orbitals.

Using the (9,12) active space we compare the spin-state energetics obtained with CASSCF, MC-PDFT and NEVPT2. Respective results are shown in Figure 5. (9,12)CASSCF yields energy gaps of 177 kJ/mol (LS-HS) and 154 kJ/mol (IS-HS), thus overestimating both gaps in comparison to the respective MC-PDFT and NEVPT2 results, but also with respect to the likely more accurate AFQMC/CBS and (DLPNO-)CCSD(T)/CBS values. Furthermore, in comparison to all of the aforementioned methods the energetic ordering of the IS and LS state is interchanged. MC-PDFT in combination with the fully translated (ft) and translated (t) versions of the PBE functional, ftPBE and tPBE, respectively, is the only method that energetically favors the IS state over

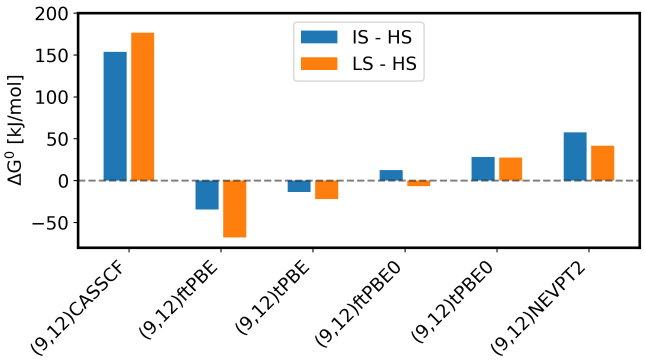

FIG. 5. Spin-state energetics of Fe(III)-NTA using different multi-reference active space methods in combination with the (9,12) active space. The basis sets used are def2-QZVPP. For further information see Figure 2.

the HS state, by 35 and 14 kJ/mol, respectively, in case of the (9,12) active space. Furthermore, (9,12)ftPBE favors the LS state more than any other method, namely by 68 kJ/mol. Like in ordinary DFT, using hybrid functionals enlarges the respective energy gaps, such that, for example, (9,12)ftPBE0 predicts 28 kJ/mol for both the LS-HS and IS-HS gaps, thus energetically favoring the HS state. However, all tested functionals within MC-PDFT favor the HS state less than their ordinary DFT counterparts, leading to MC-DFT being the largest outlier of all methods in this spin-state energetics study. It is furthermore noted that fully translated versions favor the HS less than the translated versions of the respective functionals. However, even (9,12)NEVPT2, with its more systematic inclusion of dynamic correlation within the inactive space and between active and inactive space yields energy gaps of only 42 kJ/mol (LS-HS) and 58 kJ/mol (IS-HS), which is also much lower than (DLPNO-)CCSD(T)/CBS and AFQMC/CBS, but comparable to RPA-AXK.

Figure 6 indicates that the (9,12) active space is likely not large enough to account for the most important correlations when aiming at predicting the spin-state energetics of Fe(III)-NTA, even at NEVPT2 level. Presumably, the NTA ligand requires the inclusion of additional orbitals in the active space for an accurate spin-state energetics prediction, unlike the water ligands of the hexaaqua complex studied in Ref. [50], as there the (9,12)CASSCF results with on-top perturbation theory agree well with CCSD(T) and the experimental values, differing by only 21 kJ/mol. Using DMRG-NEVPT2 based on DMRG-CASSCF for calculating the (17,20) active space, which adds the subvalence 3s and 3p orbitals, as well as their 4s and 4p virtual counterparts, to the (9,12) active space, results are obtained that are in-between (DLPNO-)CCSD(T)/CBS and AFQMC/CBS. However, in contrast to the latter two methods and the results of the other active spaces in Figure 6, (17,20)NEVPT2 favors the IS over the LS state by

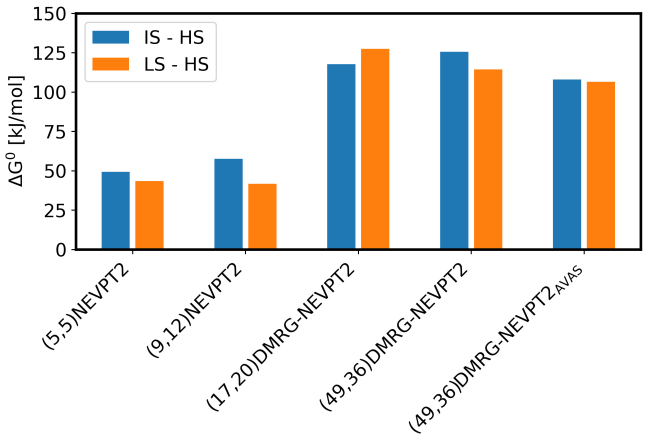

FIG. 6. Spin-state energetics of Fe(III)-NTA using the NEVPT2 method for different active spaces. The basis sets used are def2-QZVPP. The (17,20)DMRG-NEVPT2 calculation used DMRG with a MBD of 1000 both in the CASSCF and on-top NEVPT2 steps, whereas for the (49,39)DMRG-NEVPT2 calculation a MBD of 1000 was used in the CASCI step, which was based on (17,20)DMRG-CASSCF orbitals, and a reduced MBD of 600 was used in the on-top DMRG-NEVPT2 step. In case of (49,36)DMRG-NEVPT2$_{\text{AVAS}}$, the CASCI step used modified (17,20)DMRG-CASSCF orbitals based on AVAS. For further information see Figure 2.

9 kJ/mol. We verified for smaller active spaces that using DMRG as an active space solver instead of Full-CI introduces an error of less than 1 kJ/mol when using a MBD of 1000. In a recent study of multi-nuclear Fe-S compounds, Mejuto-Zaera *et al.* [161] found that a significant amount of correlation energy is only accounted for by including the Fe 3s and 3p orbitals in the active space, which is consistent with the large change (increase) of the energy gaps by 85 kJ/mol (LS-HS) and 60 kJ/mol (IS-HS) when going from the (9,12) to the (17,20) active space. However, a study by Pierloot *et al.* [36] found that NEVPT2 tends to significantly favor the LS state when including TM 3s and 3p orbitals in the active space. This does not seem to be the case here, possibly indicating that the additional inclusion of Fe 4s and 4p orbitals in the active space, something not studied by Pierloot *et al.*, might counteract this effect.

Further increasing the active space from (17,20) to (49,36) by including ligand orbitals, as described above, and running DMRG-NEVPT2 (MBD of 600) based on a DMRG-CASCI (MBD of 1000) which uses the previously optimized (17,20)DMRG-CASSCF orbitals, changes the energy gaps by at most 14 kJ/mol and again energetically favors the LS over the IS state in accordance with results obtained with the (5,5)NEVPT2 and (9,12)NEVPT2 as well as (DLPNO-)CCSD(T)/CBS and AFQMC/CBS. It is noted that the impact of reducing the MBD in the DMRG-NEVPT2 step from 1000 to 600 is expected to be very small, as a further reduction of the MBD to 400 changes the energetics by at most 1.3 kJ/mol, see section E in the Appendix. Since the (49,36)DMRG-NEVPT2 calculations were based on DMRG-CASCI instead of DMRG-CASSCF, and thus the choice of initial orbitals for the DMRG-CASCI calculation can influence the final result, we tested two variations. First, we used the natural orbitals of the (17,20)DMRG-CASSCF calculation directly, and second, we applied the modification of the AVAS method as described in section II B 5 to those orbitals to provide a different set of initial orbitals. The latter choice, which we denote as (49,36)DMRG-NEVPT2$_{\text{AVAS}}$, leads to a reduction in the energy gaps (by at most 17 kJ/mol) compared to the former choice. Nevertheless, both results are again in-between the (DLPNO-)CCSD(T)/CBS and AFQMC/CBS values.

The absolute differences between the NEVPT2 and the respective CASSCF/CASCI energy gaps decrease with increasing size of the active space, e.g. the NEVPT2 correction to CASSCF amounts to between 212 (IS-HS) and 306 kJ/mol (LS-HS) for the (5,5), to between 96 (IS-HS) and 135 kJ/mol (LS-HS) for the (9,12), to at most 53 kJ/mol for the (17,20) and to at most 30 kJ/mol for the (49,36) active space, see also section E in the Appendix. This implies that the largest active spaces in our study account well for the most important correlations when targeting the prediction of the spin-state energetics of Fe(III)-NTA.

5. *Overall Comparison Of Methods and Summary*

Of all the methods investigated for the prediction of the spin-state energetics of Fe(III)-NTA, CCSD(T), DLPNO-CCSD(T), (49,36)DMRG-NEVPT2$_{\text{AVAS}}$ and M06-L agree remarkably well on the LS-HS energy gap, which is predicted to be between 94 and 105 kJ/mol. The IS state is predicted to be at most 11 kJ/mol higher in energy than the LS state. (49,36)DMRG-NEVPT2 and AFQMC – the latter using the likely less accurate (2,3)CBS extrapolation in comparison to the (3,4)CBS extrapolation in case of DLPNO-CCSD(T) – both predict somewhat larger energy gaps of up to 139 ± 2 kJ/mol for LS-HS and up to 146 ± 2 kJ/mol for IS-HS. The great agreement between these methods, which are also deemed to be relatively reliable for the simulation of TM compounds within certain boundaries, is a strong indication that the HS state is energetically significantly favored. However, without experimental data at hand, it is not possible to conclusively favor any of these methods over one another. Furthermore, in particular the agreement of the single-reference method (DLPNO-)CCSD(T) with different methods, that are in principle capable of correctly describing multi-reference systems, such as NEVPT2 and AFQMC, is remarkable, as multi-reference diagnostics indicate that single-reference calculations may not be appropriate, at least for the IS and LS states. However, as Radoń *et al.* [50] showed for the spin-state energetics of TM-hexaaqua complexes, the good performance of single-reference CCSD(T) is not un-

Ion	$\Delta_f G^0$(Experiment) [kJ/mol]
Fe(III)	-90.8
Mn(II)	-42.2
Fe(II)	-50.2
Co(II)	-58.8
Ni(II)	-65.6
Cu(II)	-74.8

TABLE III. Experimental Gibbs free energies of formation, $\Delta_f G^0$, of TM-NTA complexes in aqueous solution in the standard state. The log$K$ values are taken from Ref. [54] (Tables 7 and 8) and the respective Gibbs free energies obtained via $\Delta_f G^0 = -RT\ln(10^{\log K})$ at $T = 298.15\,\mathrm{K}$. The experimental $\Delta_r G^0$ of Equation 1 can then be obtained via the differences in $\Delta_f G^0$ between TMs M_1 and M_2. The order of M_1 and M_2 is chosen in such a way that $\Delta_r G^0$ is always positive.

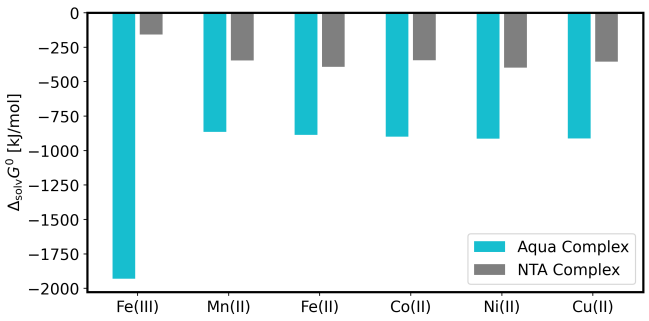

FIG. 7. Gibbs free energies of solvation, $\Delta_{solv}G^0$, for all compounds in this study using the COSMO-RS approach in aqueous solution and assuming a HS state. For further details see section II C.

precedented. The energy gaps obtained with the aforementioned methods are in some contrast to the DFT results that favor the HS state less significantly over the other spin states, namely by below 76 kJ/mol (r^{2}SCAN, TPSSh, B3LYP, PBE0, ωB97M-V), which is also the case for RPA(-AXK) as well as NEVPT2 with smaller active spaces such as (9,12) and (5,5). Even more severely, some density functionals, in particular those with no HF exchange, even favor the LS over the HS state (BP86, PBE, TPSS, DM21) including MC-PDFT ((9,12)ftPBE, (9,12)tPBE and (9,12)ftPBE0). Edler and Stein, who also investigate the effect of varying the amount of HF exchange of the B3LYP(X% HF) functional for an Fe(III) complex, find that X between 8% and 16% is optimal, [118], while in this case a much larger value of between 30% and 40% agrees with the potentially most accurate methods in our study best.

B. Selectivity of NTA

After comparing the various electronic-structure methods for the spin-state energetics of the Fe(III)-NTA complex, we now evaluate their ability to predict the selectivity of NTA with respect to six different first-row TM ions by means of comparing the respectively calculated Gibbs free energies, $\Delta_r G^0$, see Equation 1, to experimental data. For experimental data and further information see Ref. [54] and Table III.

In the previous section, we show that within DFT non-hybrid (meta-)GGA functionals such as BP86 tend to underestimate the stability of the HS state. Despite this bias, using BP86 for the calculation of the spin-state energetics of all additionally relevant TM-NTA and TM-hexaaqua complexes besides Fe(III)-NTA studied in the previous section, the HS state is always energetically favored, see Table VI in the Appendix. To safeguard against possible functional bias, we also calculated the spin-state energetics with B3LYP which confirmed that the HS state is energetically favored in all cases. This is taken as a strong indication that HS configurations and respectively optimized structures can be assumed for the calculation of the selectivity. As a further prerequisite, the amounts of water molecules that need to be explicitly taken into account in the first coordination sphere of the TM-NTA complexes were determined at the B3LYP level according to Equation 2 to be two for the NTA complexes of Fe(III), Mn(II), Fe(II), and Ni(II) and one for the NTA complexes of Co(II) and Cu(II), see Table V in the Appendix.

In order to compare the energies of different electronic-structure methods to the aforementioned experimental data in aqueous solution, those calculated electronic-structure energies need to be translated into respective Gibbs free energies in solution. In Figure 7 the Gibbs free energies of solvation, $\Delta_{solv}G^0$, are shown for all compounds at the COSMO-RS level. These energy contributions are constant for each compound and are simply added to the respective electronic-structure energies to yield Gibbs free energies in solution and from those also $\Delta_r G^0$ for the considered reactions. As a consequence, any deviation from the experimental values due to inaccuracies in the solvation treatment would result in a systematic shift of the calculated $\Delta_r G^0$ for all electronic-structure methods. In Figure 7 it can be seen that for compounds with equal charges, the magnitude of the solvation effects is comparable. Thus, they roughly cancel out when calculating reactions among those equally charged compounds. For the two Fe(III) compounds, solvation effects are quite different to those of the other systems due to different charges. Whereas Fe(III)-hexaaqua is threefold negatively charged and consequently exhibits a large $\Delta_{solv}G^0$, Fe(III)-NTA is neutral, thus exhibiting a comparably small $\Delta_{solv}G^0$. As a consequence, the final $\Delta_r G^0$ of reactions according to Equation 1 involving Fe(III) as one TM ion include relatively large solvation contributions.

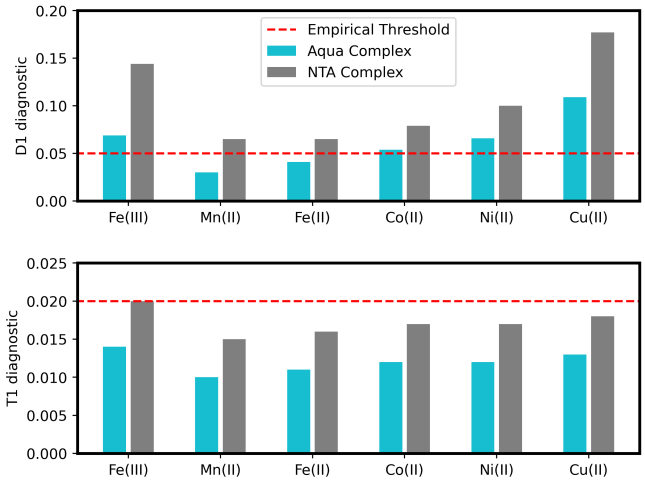

FIG. 8. Multi-reference diagnostics for all compounds in this study at the CCSD/def2-TZVP level using a ROHF orbitals and assuming a HS state. The empirical thresholds to divide into single- and multi-reference systems are shown and amount to 0.05 for D1 [160] and 0.02 for T1. [159]

1. *Multi-Reference Diagnostics*

Two of the most common multi-reference diagnostics, the D1 and the T1 diagnostic, were used to evaluate the multi-reference character of the investigated compounds. The results are shown in Figure 8. Assuming a threshold of 0.05, [160] the D1 diagnostic indicates multi-reference character for all TM-NTA complexes and all but two TM-hexaaqua complexes (Mn(II)- and Fe(II)-hexaaqua), reaching a maximum value of 0.18 for Cu(II)-NTA and a minimum value of 0.03 for Mn(II)-hexaaqua. Amongst the dicationic TMs, there is a clear trend that the D1 diagnostic increases with increasing filling of the 3d orbitals. This trend also appears for the T1 diagnostic, but is significantly less pronounced. In contrast to the D1 diagnostic, the T1 diagnostic classifies all compounds to be single-reference systems, although the maximum T1 diagnostic value, which is reached for Fe(III)-NTA, is at the empirical threshold of 0.02 given by Lee and Taylor. [159] The NTA complexes consistently show larger diagnostics than their hexaaqua counterparts. Overall, all of these insights together do neither clearly point towards a need for multi-reference electronic-structure methods to calculate reactions involving the HS NTA- and hexaaqua-complexes of the investigated first-row TM ions, nor do they clearly indicate that using single-reference electronic-structure methods is appropriate. Thus, in the following sections we evaluate the accuracy of different single- and multi-reference methods for the prediction of the selectivity of NTA with respect to different TM ions according to Equation 1 by comparing the computed $\Delta_r G^0$ to experimental data. [54]

2. *Density Functional Theory*

In Figure 9, the results obtained with eleven different density functionals are shown. With a root mean square error (RMSE) with respect to the experiment of around 19 kJ/mol, both GGA functionals BP86 and PBE and the meta-GGA functional TPSS are the worst performing density functionals of the group. The remaining two meta-GGA functionals M06-L and r^{2}SCAN, as well as the hybrid functional TPSSh, have a RMSE between 15 and 17 kJ/mol. The better performing functionals are the hybrid functionals B3LYP and M06-2X with a RMSE of around 12 kJ/mol, while the hybrid functional PBE0 and the range-separated hybrid functional ωB97M-V are the best performing density functionals with a RMSE of approximately 10 and 9 kJ/mol, respectively. While DM21 also shows a RMSE of slightly below 10 kJ/mol, it should be noted that for this functional, the compounds containing Mn(II) did not converge, and therefore the respective plot as well as the RMSE are missing 5 data points involving Mn(II). For a fairer comparison, removing these data points from the other statistics lowers their RMSE as well. However, even with these removals, DM21 with an RMSE of 10 kJ/mol still outperforms all GGA and meta-GGA functionals as well as TPSSh, where the revised RMSE falls between 13and 15 kJ/mol, and performs similarly to B3LYP at 10 kJ/mol. PBE0, M06-2X and ωB97M-V all have a revised RMSE of under 8.0 kJ/mol.

The maximum absolute error (MaxAE) was generally slightly less than twice the RMSE for all functionals, with no significant outliers. Non-hybrid functionals in general had the MaxAE from the reaction involving Fe(III) and Mn(II), except r^{2}SCAN, which along with most hybrid functionals struggled most with the reaction involving Fe(III) and Ni(II). Only the M06-2X functional had its MaxAE from a reaction not involving Fe(III), namely the Co(II)/Mn(II) reaction.

Only three functionals, namely M06-2X, ωB97M-V and DM21 do not generally overestimate $\Delta_r G^0$ for most reactions. This overestimation of all other functionals becomes particularly evident for reactions involving two TM ions that have relatively large differences in experimental selectivity, i.e. a large experimental $\Delta_r G^0$, see Figure 9. This overestimation is at least partly the reason why some of these functionals exhibit larger RMSEs. Inclusion of HF exchange appears to reduce or even flip this effect, as with an increasing amount of HF the computed $\Delta_r G^0$ of these outliers is reduced, until for M06-2X with 56% HF exchange even a slight underestimation is reached. Only the range-separated hybrid functional ωB97M-V appears to provide a rather balanced view that is not skewed in either direction.

Dispersion correction mostly plays a role for the reactions involving either Co(II) or Cu(II) (but not both), where an extra separate water molecule needs to be included on one side of the reaction to balance the stoichiometry, as the Co(II)- and Cu(II)-NTA complexes

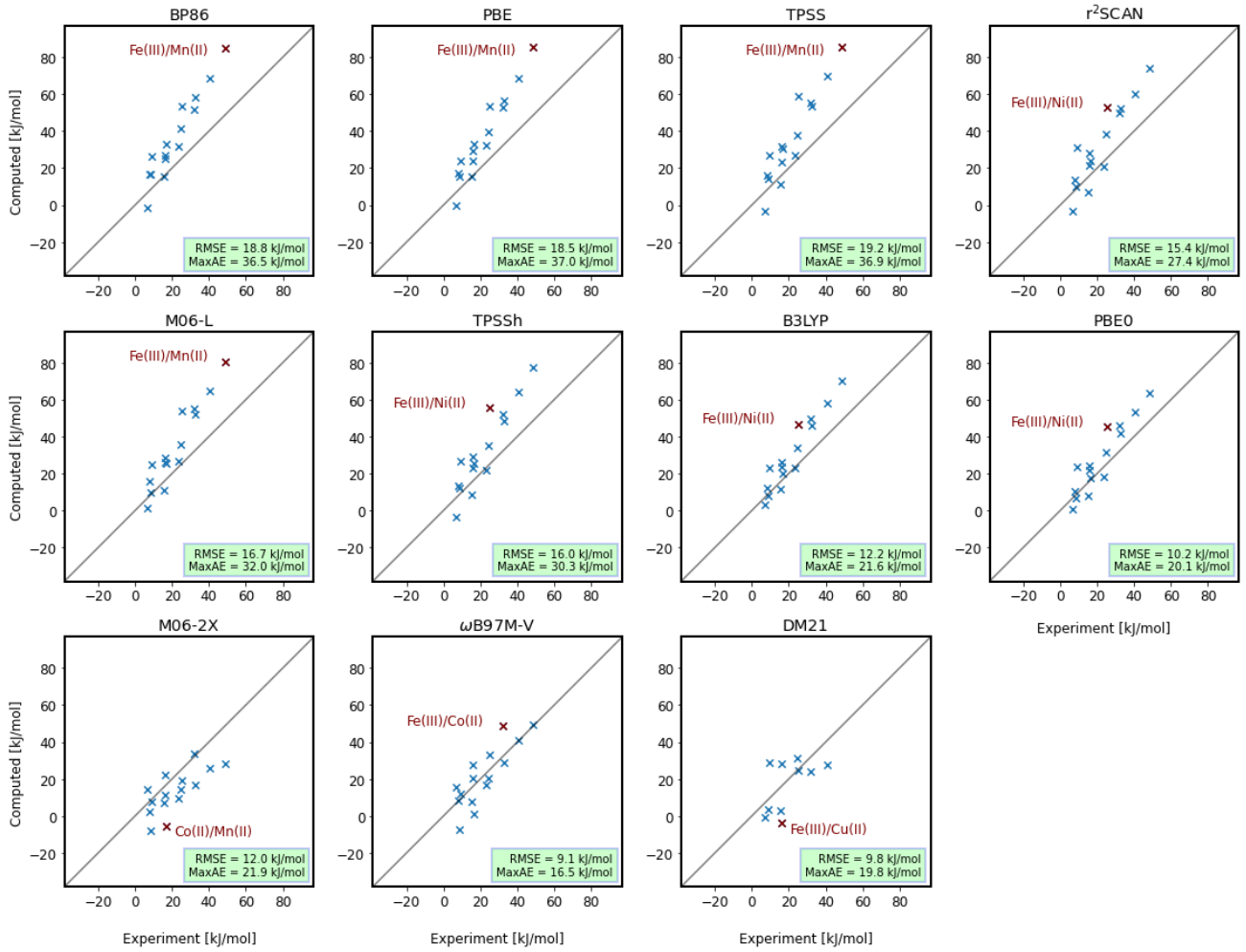

FIG. 9. Computed Gibbs free energies, $\Delta_r G^0$, using different DFT functionals for the selectivity of NTA with respect to six different TM ions according to Equation 1, plotted against the respective experimental values. The basis sets used are def2-QZVPP. The diagonal indicates perfect agreement between computed and experimental values. The root mean square error (RMSE) and maximum absolute error (MaxAE) with respect to the experiment are given, and the reaction causing the MaxAE is highlighted. In case of the DM21 functional the data points involving Mn(II) are missing, as respective calculations did not converge.

include one less explicit water molecule than the other NTA complexes. As a consequence, the dispersion correction amounts to around 12 kJ/mol for the reactions involving either Co(II) or Cu(II) and almost cancel out for all other reactions (at most 1 kJ/mol). Neglecting the D3(BJ) dispersion correction leads to RMSEs that are about 5 kJ/mol larger in case of BP86, B3LYP, and DM21 whereas for the Minnesota functionals, all without BJ damping, the RMSEs change by less than 1 kJ/mol. In no case does the inclusion of dispersion correction increase the RMSEs, while it is reduced by at least 3 kJ/mol in seven functionals.

In summary and very generally, DFT performs relatively well for the prediction of the selectivity of NTA with respect to different first-row TM ions. A DFT study by Determan *et al.* of a much broader range of first-row TM compounds found that the best functionals will give a RMSE of over 50 kJ/mol for enthalpies of formation, while for a subset of 19 compounds with lower multi-reference character and particularly reliable experimental data, the most accurate functional (B97-1) still exhibits a RMSE of 18 kJ/mol, while B3LYP for comparison shows a RMSE of 33 kJ/mol. [12] As our study is focused on a more narrow range of relatively simple reactions of first-row TM compounds occurring in their HS states, it is not surprising that these are described more accurately by DFT, in particular when using hybrid functionals. [11] However, as shown in section III A, in the context of the spin-state energetics of Fe(III)-NTA, for LS states, DFT will likely perform significantly worse.

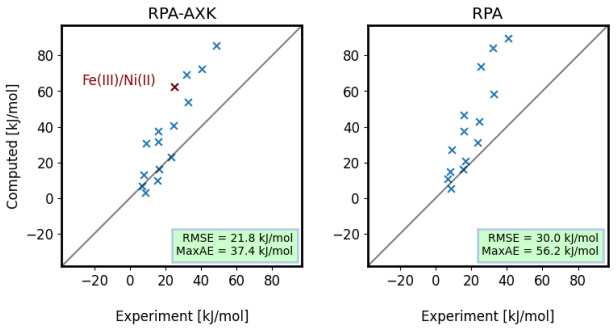

FIG. 10. Computed Gibbs free energies, $\Delta_r G^0$, using RPA with and without the AXK correction for the selectivity of NTA with respect to six different TM ions, plotted against the respective experimental values. The basis sets used are def2-QZVPP. In case of RPA, the data point with the MaxAE at (48.0, 104.9) for Fe(III)/Mn(II) is not shown. For further information see Figure 9.

3. *Random-Phase Approximation*

In Figure 10, the results obtained with RPA with and without the AXK correction are shown. In comparison to all single-reference methods and DFT functionals investigated in this study, RPA shows the largest RMSE which amounts to 30 kJ/mol and the largest MaxAE of 56 kJ/mol, which stems from the isoelectronic Fe(III)/Mn(II) reaction. Virtually all computed $\Delta_r G^0$ overestimate the respective experimental results. Adding the AXK correction improves on RPA significantly, reducing the RMSE by 8 kJ/mol as well as the MaxAE by 19 kJ/mol which now results from the Fe(III)/Ni(II) reaction, with the deviation of Fe(III)/Mn(II) being very close. Even so, the RMSE of RPA-AXK is almost 3 kJ/mol larger than the RMSE of the worst performing DFT functional, TPSS. This is rather unexpected as RPA(-AXK) is known to typically perform relatively well for small-gap systems such as first-row TM compounds. [162] Since the TPSS functional was used to generate the necessary Kohn-Sham reference for RPA, it should be noted that the two reactions exhibiting the largest errors are the identical in case of TPSS and RPA(-AXK). However, RPA(-AXK) actually exhibits larger errors than plain TPSS. This is in contrast to the performance of RPA(-AXK) for the investigation of the spin-state energetics of Fe(III)-NTA, see section III A, where RPA(-AXK) improved upon the TPSS results, yet was also a rather poorly performing method in comparison to the other investigated methods.

4. *Coupled Cluster and Møller-Plesset Perturbation Theory*

The top row of Figure 11 compares the results obtained with UHF and MP2 based on UHF molecular orbitals. MP2 greatly improves upon UHF and actually ranks among the better performing methods in this study with a RMSE of 10 kJ/mol and a MaxAE of 21 kJ/mol. The agreement of MP2 with the experiment is better than for almost all DFT functionals, with PBE0, ωB97M-V, and DM21 being the only exceptions, which are all very close to MP2. Changing to the SCS-MP2 or SOS-MP2 flavors has a negligible effect on the results, with the RMSE changing by less than 1 kJ/mol.

In the subsequent rows of plots, the results obtained with CCSD(T) in various forms are compared, which all perform very well and rank among the best performing methods in this study. In the second row of Figure 11, both the CCSD(T) and DLPNO-CCSD(T) results using the smaller def2-TZVP basis are shown, as this is the largest basis set we could afford to run CCSD(T) without the DLPNO approximation. CCSD(T)/def2-TZVP, with a RMSE of 10 kJ/mol and a MaxAE of 17 kJ/mol, yields a comparable accuracy as MP2 and the best performing DFT functionals in the def2-QZVPP basis. Like many DFT functionals, CCSD(T) also appears to overestimate the $\Delta_r G^0$, however to a significantly lesser extent. Comparing CCSD(T) to DLPNO-CCSD(T) using the def2-TZVP basis sets in both cases allows to estimate the error introduced by the DLPNO approximation. Counterintuitively, using the DLPNO approximation the RMSE and the MaxAE are lowered by 2 kJ/mol, which is at least partly due the DLPNO approximation counteracting the aforementioned overestimation of $\Delta_r G^0$. Thus, the DLPNO error is significantly smaller here than in case of the spin-state energetics of Fe(III)-NTA, see section III A 3.

The bottom row of Figure 11 shows the DLPNO-CCSD(T) results based on HF and TPSS molecular orbitals at the CBS limit using a (3,4)CBS extrapolation. The variant based on TPSS molecular orbitals is denoted DLPNO-CCSD(T)$_{\mathrm{TPSS}}$/CBS. We note that, for both variants, the respective def2-QZVPP results are already very close with a difference in the RMSE of less than 0.1 kJ/mol to the respective CBS results, see Figure 20 in the Appendix. Of all methods investigated in this study, DLPNO-CCSD(T)/CBS (and also DLPNO-CCSD(T)/def2-QZVPP) is the most accurate method with a RMSE of 5 kJ/mol and a MaxAE of 10 kJ/mol. This is also in line with the good performance of (DLPNO-)CCSD(T) in case of the spin-state energetics of Fe(III)-NTA, see section III A, and related works by Radoń *et al.* [50–52] Lastly, using DFT (TPSS) instead of HF molecular orbitals in the DLPNO-CCSD(T) calculation leads to inferior results with almost twice as large RMSE (9 kJ/mol) and MaxAE (18 kJ/mol). However, DLPNO-CCSD(T)$_{\mathrm{TPSS}}$/CBS still ranks among the better performing methods, outperforming most DFT functionals (including TPSS). Interestingly, using TPSS instead of HF molecular orbitals within DLPNO/CCSD(T) the aforementioned overestimation of $\Delta_r G^0$ reappears to some extent, which is likely due to TPSS itself exhibiting a strong overestimation whereas HF strongly underestimates the respective values.

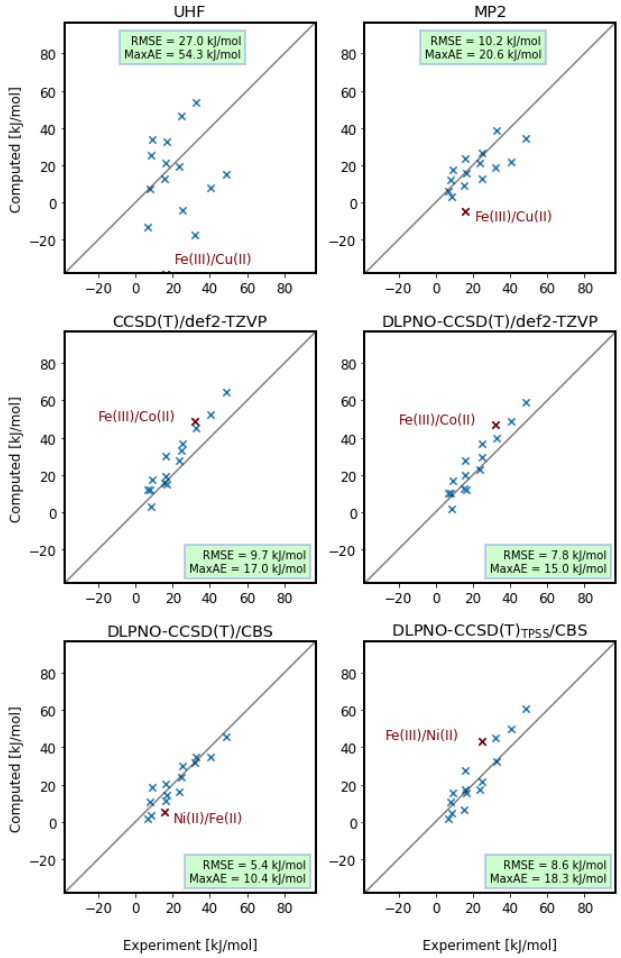

FIG. 11. Computed Gibbs free energies, $\Delta_r G^0$, using UHF, MP2, and CCSD(T) for the selectivity of NTA with respect to six different TM ions, plotted against the respective experimental values. If not indicated otherwise, the basis sets used are def2-QZVPP. In case of CCSD(T) also results obtained with the DLPNO approximation and using TPSS molecular orbitals are shown. For further information see Figure 9.

For all methods discussed above, the MaxAE originated again from reactions involving Fe(III) with the exception of DLPNO-CCSD(T)/CBS. For this method, which is the most accurate method in our study, the Ni(II)/Fe(II) reaction, which only involves dicationic TMs, was responsible for the MaxAE. This can be seen as an indication that the outlier behavior of the reactions involving Fe(III), which is observed for many methods, is likely not due to experimental uncertainties or shortcomings in the solvation model, COSMO-RS, since such sources of error would manifest as constant shifts in $\Delta_r G^0$ across all methods.

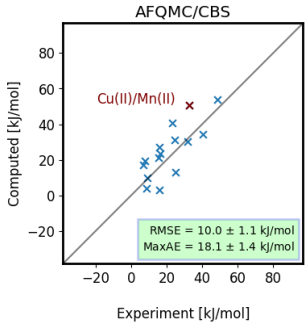

FIG. 12. Computed Gibbs free energies, $\Delta_r G^0$, using AFQMC for the selectivity of NTA with respect to six different TM ions, plotted against the respective experimental values. The (2,3)CBS extrapolation is used. As the statistical error of the AFQMC results is below 2 kJ/mol for each data point, error bars are not drawn. For further information see Figure 9.

5. *Auxiliary-Field Quantum Monte-Carlo*

In Figure 12, the results obtained with AFQMC are shown. Respective calculations are run long enough such that the statistical error for each reaction is well below 2 kJ/mol. Thus, we will neglect this error in the following discussion. The AFQMC calculations in the def2-TZVP basis sets are the computationally most expensive calculations in this study in terms of computation time. Consequently, as it was not feasible to use a larger basis sets, we had to rely on a (2,3)CBS extrapolation, as described in section A in the Appendix, which will likely introduce some additional errors in comparison to the (3,4)CBS extrapolation that we could afford in case of DLPNO-CCSD(T). In the def2-TZVP basis set, AFQMC exhibits a RMSE of 13 ± 1 kJ/mol and a MaxAE of 23 ± 2 kJ/mol, see Figure 22 in the Appendix, which is slightly worse than the respective RMSE (by 3 kJ/mol) and MaxAE (by 6 kJ/mol) of CCSD(T). The CBS extrapolation reduces the RMSE of AFQMC compared to the def2-TZVP results by more than 2 kJ/mol, and the MaxAE by more than 4 kJ/mol. The latter is obtained for the reaction involving Cu(II)/Mn(II). In the CBS limit, both the RMSE (10 ± 1 kJ/mol) and MaxAE (18 ± 1 kJ/mol) are almost twice as large in the case of AFQMC compared to DLPNO-CCSD(T). However, it needs to be emphasized again, that in case of AFQMC the less accurate (2,3)CBS extrapolation will likely be responsible for at least part of the errors. Nevertheless, AFQMC overall ranks among the better performing methods in this study with respect to accuracy, which however comes with a comparably large computational cost. The accuracy of AFQMC in this study is in line with the conclusion of Lee *et al.* that the performance of AFQMC is worse than CCSD(T), but better than CCSD, for systems where a single Slater determinant is dominant, and even for systems with some multi-reference character. [163] In section III A 3 we argued that, the AFQMC and CCSD(T) results are also

relatively close for the spin-state energetics of Fe(III)-NTA, but due to the larger multi-reference character of the LS and IS states, it is not clear that CCSD(T) should be trusted over AFQMC and it can be of great value to compare the results obtained with both complementary methods.

6. *Multi-Reference Active Space Methods*

A challenge faced in this study, that is not broadly addressed in the literature, is the use of multi-reference active space methods to calculate reaction energies. For a general chemical reaction, this leads to the additional requirement of keeping the active spaces on both sides of the chemical reaction as consistent as possible. Any chemical effects, e.g. a certain bonding situation, that are accounted for in the active space on one side of the reaction, but are accounted for only in the inactive space on the other side of the reaction, can lead to significant errors in the computed reaction energies. Recently, Bensberg and Reiher [164] proposed an automated method of selecting consistent active spaces along a chemical reaction path, expanding on earlier work. [77] However, we did not explore these techniques, as they would require each side of reaction Equation 1 to be treated in a single active space calculation with two active sites. This effectively doubles the size of the active spaces, making some calculations impractical.

Considering the selectivity of NTA and the associated chemical reaction, the difference in the general bonding situation on both sides of the chemical reaction should be rather small, as they only differ by an interchange of the central TM ions. This should lead to relatively similar molecular orbitals on both sides of the chemical reaction, thus facilitating the selection of consistent active spaces in comparison to many other imaginable chemical reactions. In the following, we compare the results obtained with active spaces of increasing size as well as different active space selection techniques. Furthermore, it will be shown that still challenges remain even for such comparably simple chemical reactions.

a. Minimal Active Spaces Since all studied systems contain one central 3d TM ion, the minimal active space comprises 5 molecular orbitals of predominantly TM 3d character. These will naturally also include all singly-occupied molecular orbitals. The outcome of a CASSCF calculation using this minimal active space does not yet depend on the initial molecular orbitals or the selection technique (within reason), as convergence to identical results is obtained regardless if starting from ROHF orbitals, UHF or UMP2 natural orbitals, or orbitals generated with the AVAS approach.

These minimal active spaces of N electrons in 5 orbitals, where N is 5 for Fe(III) and Mn(II), 6 for Fe(II), 7 for Co(II), 8 for Ni(II) and 9 for Cu(II), will be referred to from here on out as "3d" active spaces. Respective results obtained with CASSCF, MC-PDFT (in combination with the tPBE and tPBE0 density functionals), and NEVPT2 are shown in the top row of Figure 13. The CASSCF (3d) results are very close to the respective ROHF results, which is expected for these rather small active spaces in case of HS states, as the Full-CI solutions of the respective active spaces contain relatively few Slater determinants with a single (ROHF) Slater determinant being dominant in each case. Thus, it is also not surprising that CASSCF (3d) exhibits a large RMSE of 29 kJ/mol and MaxAE of 58 kJ/mol, and all reactions are within 2 kJ/mol of the respective ROHF results.

MC-PDFT (3d) using the tPBE and tPBE0 functionals produces results that are in between the respective PBE and PBE0 results, i.e. while PBE is less accurate than tPBE (3d) (RMSE of 15 kJ/mol and MaxAE of 26 kJ/mol), PBE0 is more accurate than tPBE0(3d) (RMSE of 18 kJ/mol and MaxAE of 34 kJ/mol). Interestingly, the pure tPBE (3d) and ftPBE (3d) results are more accurate than the the hybrid tPBE0 (3d) and ftPBE0 (3d) results, which is in contrast to PBE and PBE0. The translated (t) functionals match the experimental results slightly better than the fully (ft) translated functionals, however, only differing by about 2 kJ/mol in terms of RMSE, see Figure 23 in the Appendix.

NEVPT2 (3d) produces a result that – while it is a big improvement over CASSCF (3d) – is less accurate than MP2 based on ROHF (RMSE and MaxAE larger by roughly 5 and 15 kJ/mol, respectively). Although the dynamic correlation treatment in NEVPT2 is not equivalent to MP2, this difference is likely at least partly due to the fact that the used NEVPT2 implementation in `PySCF` does not allow for frozen core orbitals. For a fairer comparison, correlating all orbitals in MP2 as well, i.e. no frozen core orbitals, increases the MP2 RMSE to 14 kJ/mol and the MaxAE to 30 kJ/mol bringing it closer to the NEVPT2 (3d) results.

b. Double d-Shell Active Spaces A standard technique to expand the minimal active space is the so-called double d-shell approach, which includes adding 5 unoccupied molecular orbitals of predominantly TM-4d character to the active space, resulting in active spaces of N electrons in 10 orbitals. We will refer to this active space as "3d4d". The effect when increasing the active space from 3d to 3d4d on the CASSCF, MC-PDFT and NEVPT2 results is rather small and at most 3 kJ/mol on the RMSE and MaxAE with a minimal tendency towards a worsening of the results when expanding the active space. It is noted that attempts to further expand the 3d4d active spaces by adding σ-bonding orbitals between TM and ligand to the active space, which would result in active spaces with $N+4$ electrons in 12 orbitals, analogously to the (9,12) active space for Fe(III)-NTA in section III A, failed due to the resulting active spaces being inconsistent along most chemical reactions. Respective calculations revealed very large errors with respect to the experimental values.

In the case of NEVPT2 (3d4d), a notable group of

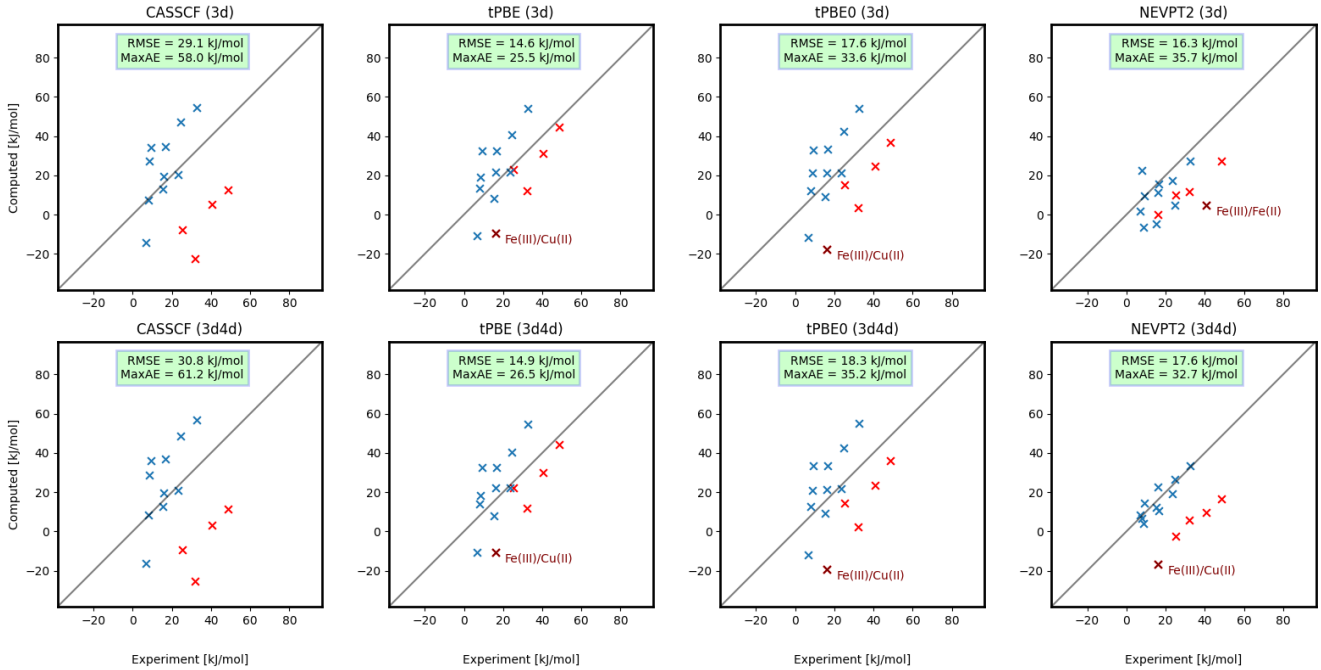

FIG. 13. Computed Gibbs free energies, $\Delta_r G^0$, using the active space methods CASSCF, MC-PDFT (in combination with the tPBE and tPBE0 density functionals), and NEVPT2 for the selectivity of NTA with respect to six different TM ions, plotted against the respective experimental values. The active spaces, abbreviated as "3d" and "3d4d" are defined in the text. The basis sets used are def2-QZVPP. In case of CASSCF (3d) and CASSCF (3d4d), the data points with the MaxAE at (16.0,-42.0) and (16.0,-45.2), respectively, for Fe(III)/Cu(II) are not shown. The reactions involving Fe(III) are highlighted in red unless they coincide with the reaction causing the MaxAE. For further information see Figure 9.

outliers can be found. This group contains all reactions involving Fe(III) and are highlighted in red in Figure 13: their computed $\Delta_r G^0$ are approximately $30-35\,\mathrm{kJ/mol}$ lower than the experimental values in case of NEVPT2 (3d4d). Without these outliers, the RMSE of the method would be a mere $4\,\mathrm{kJ/mol}$, and the MaxAE only $7\,\mathrm{kJ/mol}$, thus outperforming any other method with respect to accuracy including (DLPNO-)CCSD(T), see Figure 25 in the Appendix. These outliers imply either that the NEVPT2 (3d4d) energy for Fe(III)-NTA is too high, or the energy of Fe(III)-hexaaqua too low, or a mixture of both. This effect is also present in case of the 3d active space as well as for CASSCF and MC-PDFT, however somewhat more ambiguously, as these methods are also less accurate for the reactions not involving Fe(III). However, in case of MC-PDFT (tPBE and tPBE0), shifting the energy of Fe(III)-hexaaqua by roughly $+30\,\mathrm{kJ/mol}$ or, alternatively, shifting the energy of Fe(III)-NTA by $-30\,\mathrm{kJ/mol}$, would make respective plots look remarkably similar to those of DFT with the PBE and PBE0 functionals, where the computed $\Delta_r G^0$ of the reactions involving Fe(III) are generally larger than the experimental values. This would also explain the dissonance between hybrid functionals having a larger RMSE than non-hybrid functionals within MC-PDFT, while within DFT this trend is reversed. While PBE overestimates $\Delta_r G^0$ for many reactions, this overestimation is partly compensated for in case of tPBE and ftPBE by this "systematic" shift of all reactions involving Fe(III) towards smaller $\Delta_r G^0$. Since PBE0 is already closer to the experimental value, the aforementioned "systematic" shift rather leads to an overcompensation and thus larger errors in case of tPBE0 and ftPBE0.

It is not clear what causes this behavior of the reactions involving Fe(III). Great care was taken to make sure that this effect is not due to any technical issues in the calculations, e.g. convergence to an incorrect state. Inaccuracies due to the solvation model, COSMO-RS, as discussed with respect to Figure 7, are possible due to the different charge of the Fe(III) compounds compared to all other compounds, but would manifest as constant shifts in $\Delta_r G^0$ across all methods. Furthermore, the very good agreement of DLPNO-CCSD(T)/CBS with the experimental data makes errors in the latter rather unlikely. In section D in the Appendix, we examine in more detail another possible source of error, namely the qualitatively different geometrical structure of Fe(III)-hexaaqua compared to the other (dicationic) TM-hexaaqua complexes, which is likely due to the solvation treatment at the COSMO level in the structure optimization. However, repeating NEVPT2 (3d4d) assuming a modified structure of Fe(III)-hexaaqua with the same symmetry as the other TM-hexaaqua complexes even leads to further deviations from the experimental Gibbs free energies.

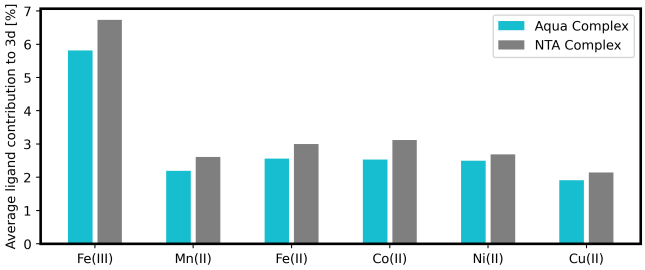

FIG. 14. Average contribution of ligand atomic orbitals to the nominally TM 3d molecular orbitals for all compounds using a Mulliken population analysis after a CASSCF (3d4d) calculation. The basis set used is def2-QZVPP.

Perhaps the most likely explanation for the outlier behavior of the reactions involving Fe(III) is simply an inconsistency in the 3d and 3d4d active spaces between the Fe(III)-containing and all other compounds. A closer look at the atomic orbital contributions to the nominally TM 3d molecular orbitals by means of a Mulliken population analysis after a CASSCF (3d4d) calculation reveals that the five 3d molecular orbitals of the Fe(III)-containing compounds have more than twice as much ligand atomic orbital contributions than the 3d molecular orbitals of the other (dicationic) TM ions. For example, the average Fe 3d molecular orbital in Fe(III)-NTA is a linear combination of 93% Fe 3d atomic orbital and 7% O 2p and N 2p ligand atomic orbitals, see Figure 14, whereas for all other TM-NTA compounds the contribution of ligand atomic orbitals amounts to only between 2 and 3%. A similar trend is observed when comparing Fe(III)-hexaaqua to the other TM-hexaaqua compounds. In all cases, contributions from other atomic orbitals to the nominally TM 3d molecular orbitals are negligible. An analysis of the nominally TM-4d molecular orbitals reveals that the Fe(III)-containing compounds show a larger extent of mixing of the Fe-4d atomic orbitals with other Fe atomic orbitals (mostly Fe-5d and Fe-6d) than all other compounds. Additionally, the natural orbital occupation numbers from the CASSCF (3d4d) calculations of the nominally Fe-4d molecular orbitals are smaller (around 0.002) then in case of the TM-4d molecular orbitals of all other compounds (for the isoelectronic Mn(II)-compounds around 0.004 and for others even larger).

Regardless of the reason for the outlier behavior of the reactions involving Fe(III), this investigation demonstrates both the potential as well as the challenges of multi-reference active space methods such as NEVPT2. For reactions only involving species for which selecting consistent active spaces is feasible, as in case of reactions only involving the compounds containing dicationic TMs in this study, high accuracy is often achievable with reasonably sized active spaces, so much so that NEVPT2 (3d4d) in this case would rank as the most accurate method investigated in our study, see Figure 25 in the Appendix. However, active space consistency problems can emerge, as in this case for reactions involving the Fe(III)-containing compounds, that are very hard to diagnose.

c. Semiautomatic Active Space Selection Based on Single Orbital Entropies In the following, we use the semiautomatic active space selection approach based on single-orbital entropies (SOEs) as described in section II B 5 and evaluate whether consistent active spaces for the investigated chemical reactions can be constructed, that possibly also contain orbitals beyond the 3d4d active spaces that were discussed in section III B 6 b.

In fact, the SOE approach allows for the selection of active spaces that, while not necessarily of the same size for all TM-NTA and all TM-hexaaqua complexes, do share mostly the same characteristics. This leads to the errors, i.e. the RMSE and MaxAE, to be within reasonable bounds, see top row of Figure 15.

For the TM-hexaaqua complexes, none of the orbitals (which are unrestricted MP2 natural orbitals) exhibited SOEs larger than the default threshold of 0.14 but instead SOEs of at most 0.08. As a result, the only orbitals added to the active spaces are the singly occupied TM 3d orbitals, which leads to CASSCF converging to the respective ROHF solution. This can be interpreted as a sign that, for the calculation of the TM-hexaaqua complexes, there is no need for multi-reference methods, despite the borderline D1 diagnostics.

However, for the NTA complexes, besides the singly occupied TM 3d orbitals, there are further orbitals added to the active spaces that exceed the default SOE threshold: for each TM-NTA complex, three doubly occupied (SOEs between 0.14 and 0.16) and three unoccupied orbitals (SOEs between 0.17 and 0.18) have significantly larger SOEs than the rest (at most 0.07). It is noted that we refer to them as doubly occupied and unoccupied due to their unrestricted MP2 natural occupation numbers being around 1.94 and 0.06, respectively. The doubly occupied orbitals do not contain notable contributions from atomic orbitals of the TM, even for those TM-NTA complexes that have some doubly occupied TM 3d orbitals. Rather, they are orbitals that contain large contributions from the 2p atomic orbitals of the three oxygen atoms of NTA facing away from the TM center as well as smaller contributions from the 2p atomic orbitals of the oxygen and nitrogen atoms in the first coordination sphere of the TM center. The unoccupied orbitals mostly contain in even proportion large contributions from the 3p atomic orbitals of the carbon atoms of the three carboxyl groups as well as smaller contributions from the 3p atomic orbitals of the three oxygen atoms of NTA facing away from the TM center. A possible explanation for these orbitals being selected into the active space, despite having no notable TM contributions, is the lack of solvation treatment in the single-point energy calculations. With the absence of a solvent to screen higher charge densities as found on the outward-facing oxygen atoms, the orbitals located there are raised in energy, which obviously makes

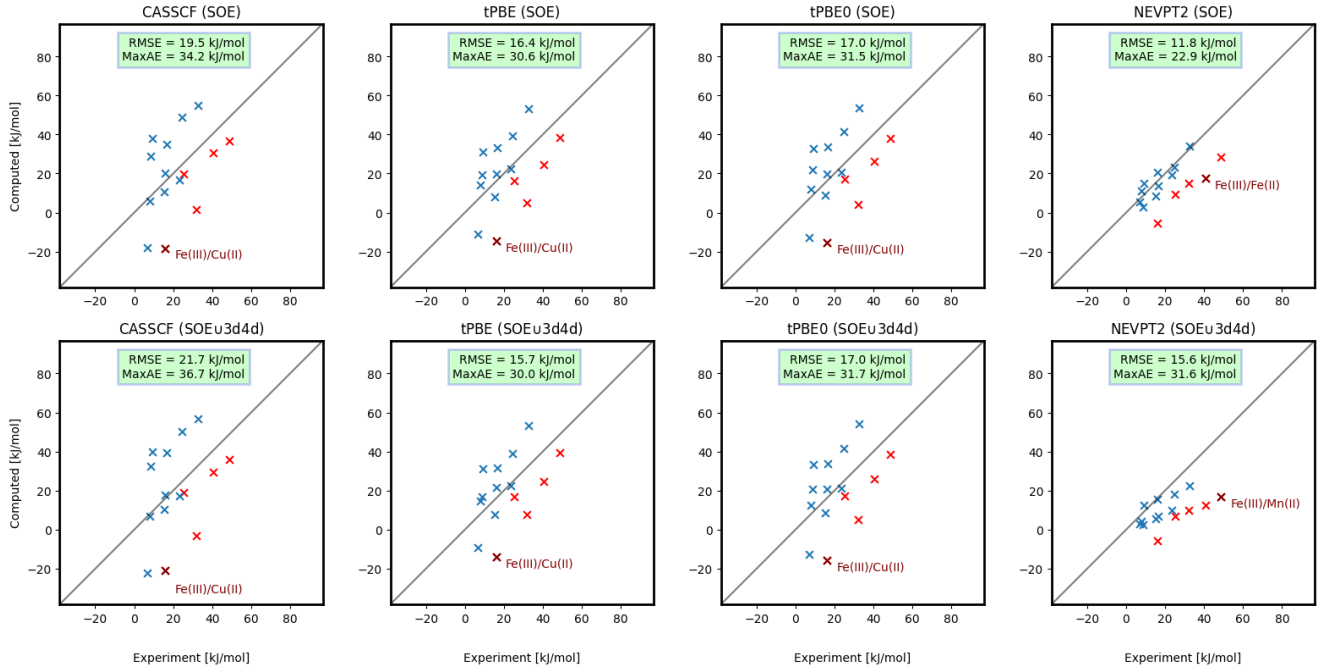

FIG. 15. Computed Gibbs free energies, $\Delta_r G^0$, using the active space methods of Figure 13, in combination with active spaces based on single-orbital entropies, "SOE", and "SOE∪3d4d", as defined in the text, for the selectivity of NTA with respect to six different TM ions, plotted against the respective experimental values. The basis sets used are def2-QZVPP. For further information see Figure 13.

them eligible for inclusion into the active space. However, this semiautomatic active space selection technique is able to identify ligand orbitals at NTA that i) are not obvious candidates for the active space by other metrics, and ii) are consistent across all TM-NTA complexes.

In the top row of Figure 15 the results obtained for the aforementioned active spaces are shown, ranging from a (1,1) active space for Cu(II)-hexaaqua to a (5,5) active space for Mn(II)- and Fe(III)-hexaaqua, as well as a (7,7) active space for Cu(II)-NTA to a (11,11) active space for Mn(II)- and Fe(III)-NTA. We refer to these active spaces from hereon collectively as SOE active spaces. These active spaces describe the reactions better than the 3d and 3d4d active spaces discussed above, with a RMSE that is reduced by 10 kJ/mol (MaxAE reduced by more than 20 kJ/mol) in case of CASSCF and reduced by more than 4 kJ/mol (MaxAE reduced by more than 10 kJ/mol) in case of NEVPT2. In case of MC-PDFT the change – both an increase and decrease depending on the density functional – is less than 2 kJ/mol (MaxAE less than 5 kJ/mol), overall making MC-PDFT again rather agnostic to the choice of the specific active space, as long as it is within reason. However, also the results obtained with the SOE active space exhibit the outlier behavior of reactions involving Fe(III), but to a lesser extent, with their computed $\Delta_r G^0$ being shifted by roughly 20 kJ/mol below the experimental values in case of NEVPT2 (SOE) instead of 30 to 35 kJ/mol in case of NEVPT2 (3d4d).

We also combined the SOE active space with the previously studied 3d4d active space, which we denote as SOE∪3d4d active space. The largest of these active spaces, which occurred for Mn(II)-NTA and Fe(III)-NTA, comprise 11 electrons in 16 orbitals. Respective results are shown in the bottom row of Figure 15. In comparison to the SOE active spaces, no improvement of the results is observed. For CASSCF, both the RMSE and MaxAE slightly increase by approximately 2 kJ/mol and for MC-PDFT the changes are below 1 kJ/mol, for NEVPT2 the RMSE even increases by 4 kJ/mol and the MaxAE by almost 9 kJ/mol. In particular, in case of NEVPT2 (SOE∪3d4d) the larger errors are partly due to a further shift of the computed $\Delta_r G^0$ of the reactions involving Fe(III) and other reactions in comparison to the NEVPT2 (SOE) results.

d. Density Matrix Renormalization Group Theory for Larger Active Spaces In the following, we evaluate the impact of adding further orbitals with predominantly TM character to the 3d4d active space that was discussed in section III B 6 b. A natural choice therefore are the sub-valence 3s and 3p orbitals at the TM centers as well as their virtual counterparts, 4s and 4p. Also, the addition of these orbitals to the active spaces turned out to be important for a proper description of the spin-state energetics of Fe(III)-NTA, see section III A 4. The modification of the AVAS method as described in section II B 5 was used to select the aforementioned active

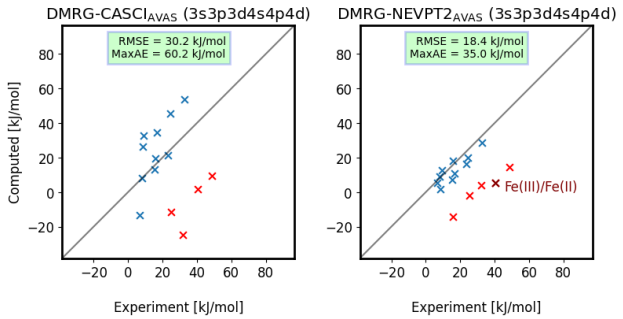

FIG. 16. Computed Gibbs free energies, $\Delta_r G^0$, using the active space methods DMRG-CASCI and DMRG-NEVPT2 for the selectivity of NTA with respect to six different TM ions, plotted against the respective experimental values. The active spaces, abbreviated as "3s3p3d4s4p4d", are defined in the text. The basis sets used are def2-QZVPP. For DMRG a MBD of 1000 was used. The CASCI step used modified CASSCF (3d4d) orbitals based on AVAS. In case of DMRG-CASCI the data point with the MaxAE at (16.0, -44.1) for Fe(III)/Cu(II) are not shown. For further information see Figure 13.

spaces, which we denote as "3s3p3d4s4p4d" active spaces, based on the CASSCF (3d4d) orbitals. The resulting active spaces comprise 18 orbitals and were solved by means of DMRG with a MBD of 1000. The respective results obtained at the DMRG-CASCI$_{AVAS}$ (3s3p3d4s4p4d) and DMRG-NEVPT2$_{AVAS}$ (3s3p3d4s4p4d) levels are shown in Figure 16. For these active spaces, using (DMRG-)CASSCF instead of (DMRG-)CASCI, i.e. carrying out further orbital optimization, was not feasible due to large inconsistencies among the resulting active spaces for the different TM-hexaaqua and TM-NTA compounds, leading to very large errors. Nevertheless, both DMRG-CASCI$_{AVAS}$ (3s3p3d4s4p4d) and DMRG-NEVPT2$_{AVAS}$ (3s3p3d4s4p4d) yield results that are virtually identical to CASSCF (3d4d) and NEVPT2 (3d4d), respectively, with changes in the RMSE of below 1 kJ/mol (MaxAE 2 kJ/mol) and persistent outlier behavior of reactions involving Fe(III).

IV. CONCLUSION

In this work we applied a full quantum-chemical workflow including structure optimization, different single-point energy methods, thermodynamics and solvation treatment to the calculation of the selectivity of the industrially relevant and chemically rather representative chelating agent nitrilotriacetic acid (NTA) with respect to six different 3d transition metal (TM) ions in aqueous solution. The focus was on assessing the quality of a large variety of single-point energy methods by comparing the computational results to experimental data. The investigated electronic-structure methods include: different DFT functionals including the deep neural network parameterized DM21 functional, RPA, MP2, CCSD(T) with and without the DLPNO approximation, and AFQMC, as well as the multi-reference active space method CASSCF in combination with the on-top methods MC-PDFT and NEVPT2. We furthermore investigated different active spaces and active space selection techniques including AVAS as well as using single-orbital entropies as selection criterion. We also applied DMRG in combination with larger active spaces. For one chelate complex, Fe(III)-NTA, we additionally studied the spin-state energetics in detail, applying the aforementioned methods, and used the results to inform our choice of multiplicity also for the other NTA complexes.

For the spin-state energetics of Fe(III)-NTA, we found that conceptually different methods, which would also *a priori* be considered to be relatively accurate for this task, [50, 51], namely the M06-L functional, (DLPNO-)CCSD(T), and DMRG-NEVPT2 in combination with the largest active space in our study containing 49 electrons in 36 orbitals, agree remarkably well and predict the high-spin (HS) state to be energetically favored over the low-spin (LS) state by between 94 and 105 kJ/mol. The intermediate-spin (IS) state was predicted to be at most 11 kJ/mol higher in energy than the LS state. As a generally very accurate method, AFQMC also agreed with this trend, but predicted the HS state to be more strongly stabilized by an additional 40 kJ/mol, likely in part due to the less accurate CBS extrapolation which we needed to rely on due to the large computational cost of the method. Overall, this was seen as a strong indication that the HS state of Fe(III)-NTA is the energetically most favorable spin state, although no experimental data was available and thus none of the investigated methods could be reliably considered optimal.

Results obtained using the most reliable multi-reference active space method in our study, (DMRG-)NEVPT2, in combination with smaller active spaces containing five Fe 3d, five Fe 4d and two σ-bonding orbitals or parts thereof yielded a significantly smaller stabilization of the HS state of at most 43 kJ/mol with respect to the LS state, which is in contrast to the spin-state energetics of Fe(III)-hexaaqua, for which the aforementioned active space already led to relatively accurate predictions. [50] The additional inclusion of the subvalence Fe 3s and 3p orbitals and their 4s and 4p virtual counterparts, resulting in a (17,20) active space, led to a two to three times larger stabilization of the HS state with respect to the LS and IS states, the latter of which were however interchanged in order. Further addition of the 2p orbitals of each ligand atom in the first coordination sphere, leading to the (49,36) active space, finally yielded results both qualitatively and quantitatively in agreement with other conceptually different methods as described above.

Similarly to NEVPT2 in combination with smaller active spaces, RPA(-AXK) and most DFT functionals also led to a comparably small stabilization of the HS

state of below 76 kJ/mol with respect to the other spin states with the exception of the Minnesota functionals M06-L and M06-2X. In agreement with previous studies, DFT results were found to be very functional-dependent with the energetic stabilization of the HS state over the other spin states increasing nearly linearly with the amount of HF exchange in the functional. [37, 118, 165–167] Most severely, in particular non-hybrid functionals (BP86, PBE and TPSS) as well as the DM21 functional and MC-PDFT even favored the LS over the HS state by up to 49 kJ/mol, thus even qualitatively disagreeing with the presumably more accurate methods discussed above.

The various electronic-structure methods were then assessed in terms of to their practical ability to predict the selectivity of NTA with respect to six different 3d TM ions which all exist in their HS state. The respectively calculated Gibbs free energies were compared to experimental data. An overview of the accuracy of all studied methods can be found in Figure 25 in the Appendix. Of all the methods studied, DLPNO-CCSD(T) – for which in contrast to CCSD(T) we could afford to use large basis sets and carry out accurate CBS extrapolations – consistently gave the best agreement with experiment across all chemical reactions, with a root mean square error (RMSE) of only 5 kJ/mol and a maximum absolute error (MaxAE) of 10 kJ/mol. AFQMC, which is also deemed to be a highly accurate method and particularly trustworthy for multi-reference systems, performed somewhat worse than DLPNO-CCSD(T) with a RMSE and MaxAE being almost twice as large, which could at least partially be attributed to a less accurate CBS extrapolation. Nevertheless, AFQMC ranked among the most accurate methods in our study.

Results obtained with DFT, which is computationally significantly cheaper, were more consistent among different functionals than in case of the spin-state energetics of Fe(III)-NTA. Of the eleven functionals tested, the range-separated hybrid functional ωB97M-V performed best and even slightly better than AFQMC with a RMSE of 9 kJ/mol and a MaxAE of 17 kJ/mol. For DM21, not all calculations converged. In agreement with Jacob's ladder, the hybrid functionals exhibited RMSEs of between 10 and 16 kJ/mol and the (meta-)GGA functionals RMSEs of between 15 and 19 kJ/mol, with the MaxAEs typically being slightly less than twice as large as the respective RMSEs in most cases. Overall, particularly the latter class of density functionals exhibited rather poor accuracy in relation to all other investigated methods. A bit surprisingly, this was even more so the case for RPA-AXK, with a RMSE of 22 kJ/mol, which is larger than that of any DFT functional and only 5 kJ/mol smaller than that of Hartree-Fock.

The application of active space methods to the selectivity of NTA came with the challenge that the active spaces on both sides of the respective chemical reactions needed to be kept consistent. In practice this limited the sizes and complexities of the active spaces, in contrast to the spin-state energetics. The results obtained with active spaces either containing only five TM 3d orbitals or additionally five TM 4d orbitals were very similar, with NEVPT2 showing an accuracy that was in between those of (meta-)GGA and hybrid DFT. Similarly, the accuracy of MC-PDFT was comparable to that of DFT. However, the unexpectedly large RMSE of NEVPT2 of between 16 and 18 kJ/mol could be traced back to a notable group of outlier reactions which involved Fe(III) and underestimated the respective experimental values by roughly 30 kJ/mol. The further addition of the 3s, 3p, 4s and 4p orbitals at the TM to the active space and application of DMRG-NEVPT2 led to virtually identical results, in contrast to the spin-state energetics. Alternatively, using active spaces that were selected based on single-orbital entropies, which led to active spaces containing only the singly occupied TM 3d orbitals for the aqua complexes and additionally six orbitals exclusively located at the NTA ligand in case of the NTA complexes, somewhat reduced this underestimation thus also reducing the RMSE to 12 kJ/mol. In fact, it was observed that the reactions involving Fe(III) were responsible for the MaxAEs in case of most of the investigated methods, including also DFT, RPA and CCSD(T). However, in case of those methods, not all reactions involving Fe(III) were shifted and the experimental values were rather overestimated. We concluded that this behavior is likely not due to experimental uncertainties or shortcomings in the solvation model, but rather due to an inconsistency in the active spaces between the Fe(III)-containing compounds and all other compounds, as for the former the nominally 3d orbitals contained significantly larger ligand atomic orbital contributions. Excluding Fe(III) from the statistics of all investigated methods actually led to NEVPT2 showing the highest accuracy of all methods with a RMSE of merely 4 kJ/mol and a MaxAE of 7 kJ/mol.

Overall, the investigated chemical reactions of chelate complexes of 3d TMs in their HS state were handled relatively well by most electronic-structure methods, indicating that most of the systems can effectively be considered as single-reference, despite ambiguous multi-reference diagnostics. The computationally rather expensive methods like single-reference (DLPNO-)CCSD(T) yielded the best accuracy. Multi-reference methods like (DMRG-)NEVPT2 were potentially even somewhat more accurate but came with the challenge of selecting consistent active spaces along the chemical reaction. However, even the much cheaper (range-separated) hybrid DFT still yielded very good accuracy. The true challenge seemed to be the simulation of the LS and IS states of the 3d TM chelate complex Fe(III)-NTA, for which DFT was no longer trustworthy. Nevertheless, single-reference (DLPNO-)CCSD(T) again agreed very well with the multi-reference methods (DMRG-)NEVPT2 and AFQMC despite several diagnostics indicating multi-reference character. However, it is not clear *a priori* if (DLPNO-)CCSD(T) would perform equally well for other systems with potential multi-reference character. Therefore, a comparison to conceptually different, highly

accurate methods, such as AFQMC which does not necessarily depend on the − often challenging − selection of an active space, can be of great value.

ACKNOWLEDGMENTS

The authors thank Oliver Welz for valuable advice on the experimental data and the use of the ORCA software. This work was supported by the German Federal Ministry of Education and Research (BMBF) within the funding program "Quantum technologies — From basic research to market" in the joint project MANIQU (Grant No. 13N15575).

[1] K. P. S. Cheung, S. Sarkar, and V. Gevorgyan, Chemical Reviews **122**, 1543 (2022).
[2] H. Yorimitsu, M. Kotora, and N. T. Patil, The Chemical Record **21**, 3335 (2021).
[3] U. B. Kim, D. J. Jung, H. J. Jeon, K. Rathwell, and S.-g. Lee, Chemical Reviews **120**, 13382 (2020).
[4] J.-M. Kim, X. Zhang, J.-G. Zhang, A. Manthiram, Y. S. Meng, and W. Xu, Materials Today **46**, 155 (2021).
[5] H. Liu, X. Liu, S. Wang, H.-K. Liu, and L. Li, Energy Storage Materials **28**, 122 (2020).
[6] J.-H. Zuo and Y.-J. Gong, Tungsten **2** (2020).
[7] A. D. Read, R. E. Bentley, S. L. Archer, and K. J. Dunham-Snary, Redox Biology **47**, 102164 (2021).
[8] P. Wang, Y. Yuan, K. Xu, H. Zhong, Y. Yang, S. Jin, K. Yang, and X. Qi, Bioactive materials **6**, 916 (2021).
[9] S. Zehra, S. Tabassum, and F. Arjmand, Drug Discovery Today **26**, 1086 (2021).
[10] S. B. Schmidt and S. Husted, Plants **8**, 381 (2019).
[11] L. R. Maurer, M. Bursch, S. Grimme, and A. Hansen, Journal of Chemical Theory and Computation **17**, 6134 (2021).
[12] J. J. Determan, K. Poole, G. Scalmani, M. J. Frisch, B. G. Janesko, and A. K. Wilson, Journal of Chemical Theory and Computation **13**, 4907 (2017).
[13] C. A. Jiménez-Hoyos, B. G. Janesko, and G. E. Scuseria, J. Phys. Chem. A **113**, 11742 (2009).
[14] E. R. Johnson and A. D. Becke, Can. J. Chem. **87**, 1369 (2009).
[15] W. Zhang, D. G. Truhlar, and M. Tang, Journal of Chemical Theory and Computation **9**, 3965 (2013).
[16] M. Bühl, C. Reimann, D. A. Pantazis, T. Bredow, and F. Neese, J. Chem. Theory Comput. **4**, 1449 (2008).
[17] F. Furche and J. P. Perdew, The Journal of Chemical Physics **124** (2006).
[18] Y. Zhao and D. G. Truhlar, The Journal of Chemical Physics **125** (2006).
[19] T. R. Cundari, Chem. Rev. **100**, 807 (2000).
[20] A. W. Ehlers and G. Frenking, J. Am. Chem. Soc. **116**, 1514 (1994).
[21] C. Sosa, J. Andzelm, B. C. Elkin, E. Wimmer, K. D. Dobbs, and D. A. Dixon, J. Phys. Chem. **96**, 6630 (1992).
[22] H. S. Yu, W. Zhang, P. Verma, X. He, and D. G. Truhlar, Phys. Chem. Chem. Phys. **17**, 12146 (2015).
[23] N. Mardirossian and M. Head-Gordon, The Journal of Chemical Physics **144** (2016).
[24] J. E. Bates, P. D. Mezei, G. I. Csonka, J. Sun, and A. Ruzsinszky, Journal of Chemical Theory and Computation **13**, 100 (2017).
[25] C. Waitt, N. M. Ferrara, and H. Eshuis, Journal of Chemical Theory and Computation **12**, 5350 (2016).
[26] J. Chedid, N. Ferrara, and H. Eshuis, Theoretical Chemistry Accounts **137**, 1 (2018).
[27] D. Hait, N. M. Tubman, D. S. Levine, K. B. Whaley, and M. Head-Gordon, Journal of Chemical Theory and Computation **15**, 5370 (2019).
[28] J. Raab and B. O. Roos, in *Advances in Quantum Chemistry*, Vol. 48 (Academic Press, 2005) pp. 421–433.
[29] A. Pulkin and G. K.-L. Chan, Phys. Rev. B **101**, 241113 (2020).
[30] A. Altun, C. Riplinger, F. Neese, and G. Bistoni, Journal of Chemical Theory and Computation **19**, 2039 (2023).
[31] P. S. Schmidt and K. S. Thygesen, The Journal of Physical Chemistry C **122**, 4381 (2018).
[32] A. Khedkar and M. Roemelt, Phys. Chem. Chem. Phys. **23**, 17097 (2021).
[33] W. Jiang, N. J. DeYonker, and A. K. Wilson, Journal of Chemical Theory and Computation **8**, 460 (2012).
[34] J. Wang, S. Manivasagam, and A. K. Wilson, Journal of Chemical Theory and Computation **11**, 5865 (2015).
[35] D. Süß, S. E. Huber, and A. Mauracher, The Journal of Chemical Physics **152** (2020).
[36] K. Pierloot, Q. M. Phung, and A. Domingo, Journal of Chemical Theory and Computation **13**, 537 (2017).
[37] L. M. Lawson Daku, F. Aquilante, T. W. Robinson, and A. Hauser, Journal of Chemical Theory and Computation **8**, 4216 (2012).
[38] M. Nakagaki and S. Sakaki, Physical chemistry chemical physics **17**, 16294 (2015).
[39] S. K. Singh, J. Eng, M. Atanasov, and F. Neese, Coordination Chemistry Reviews **344**, 2 (2017).
[40] S. K. Singh, M. Atanasov, and F. Neese, Journal of Chemical Theory and Computation **14**, 4662 (2018).
[41] T. Husch, L. Freitag, and M. Reiher, Journal of chemical theory and computation **14**, 2456 (2018).
[42] S. J. Stoneburner, D. G. Truhlar, and L. Gagliardi, The Journal of Physical Chemistry A **124**, 1187 (2020).
[43] C. Zhou, D. Wu, L. Gagliardi, and D. G. Truhlar, Journal of Chemical Theory and Computation **17**, 5050 (2021).
[44] K. H. Marti, I. M. Ondík, G. Moritz, and M. Reiher, The Journal of Chemical Physics **128**, 014104 (2008).
[45] R. Olivares-Amaya, W. Hu, N. Nakatani, S. Sharma, J. Yang, and G. K.-L. Chan, The Journal of Chemical Physics **142**, 034102 (2015).
[46] H. R. Larsson, H. Zhai, C. J. Umrigar, and G. K.-L. Chan, Journal of the American Chemical Society **144**,

15932 (2022).
[47] M. Amsler, P. Deglmann, M. Degroote, M. P. Kaicher, M. Kiser, M. Kühn, C. Kumar, A. Maier, G. Samsonidze, A. Schroeder, M. Streif, D. Vodola, C. Wever, and Q. M. S. W. Group, The Journal of Chemical Physics **159**, 044119 (2023).
[48] J. Shee, B. Rudshteyn, E. J. Arthur, S. Zhang, D. R. Reichman, and R. A. Friesner, Journal of Chemical Theory and Computation **15**, 2346 (2019).
[49] E. J. Landinez Borda, J. Gomez, and M. A. Morales, The Journal of Chemical Physics **150**, 074105 (2019).
[50] M. Radoń, K. Gąssowska, J. Szklarzewicz, and E. Broclawik, Journal of Chemical Theory and Computation **12**, 1592 (2016).
[51] M. Radoń and G. Drabik, Journal of Chemical Theory and Computation **14**, 4010 (2018).
[52] M. Radoń, Phys. Chem. Chem. Phys. **21**, 4854 (2019).
[53] X. Xu, W. Zhang, M. Tang, and D. G. Truhlar, Journal of Chemical Theory and Computation **11**, 2036 (2015).
[54] R. M. Smith and A. E. Martell, Science of The Total Environment **64**, 125 (1987), environmental Inorganic Chemistry.
[55] J. Kirkpatrick, B. McMorrow, D. H. P. Turban, A. L. Gaunt, J. S. Spencer, A. G. D. G. Matthews, A. Obika, L. Thiry, M. Fortunato, D. Pfau, L. R. Castellanos, S. Petersen, A. W. R. Nelson, P. Kohli, P. Mori-Sánchez, D. Hassabis, and A. J. Cohen, Science **374**, 1385 (2021).
[56] D. Bohm and D. Pines, Phys. Rev. **82**, 625 (1951).
[57] D. Pines and D. Bohm, Phys. Rev. **85**, 338 (1952).
[58] D. Bohm and D. Pines, Phys. Rev. **92**, 609 (1953).
[59] C. Møller and M. S. Plesset, Phys. Rev. **46**, 618 (1934).
[60] K. Raghavachari, G. W. Trucks, J. A. Pople, and M. Head-Gordon, Chemical Physics Letters **157**, 479 (1989).
[61] J. D. Watts, J. Gauss, and R. J. Bartlett, The Journal of Chemical Physics **98**, 8718 (1993).
[62] D. G. Liakos and F. Neese, Journal of Chemical Theory and Computation **11**, 4054 (2015).
[63] Y. Guo, C. Riplinger, D. G. Liakos, U. Becker, M. Saitow, and F. Neese, The Journal of Chemical Physics **152**, 024116 (2020).
[64] S. Zhang and H. Krakauer, Phys. Rev. Lett. **90**, 136401 (2003).
[65] B. O. Roos, in *Advances in Chemical Physics* (John Wiley & Sons, Ltd, 1987) pp. 399–445.
[66] M. W. Schmidt and M. S. Gordon, Annual Review of Physical Chemistry **49**, 233 (1998).
[67] C. Angeli, R. Cimiraglia, S. Evangelisti, T. Leininger, and J.-P. Malrieu, The Journal of Chemical Physics **114**, 10252 (2001).
[68] R. K. Carlson, D. G. Truhlar, and L. Gagliardi, Journal of Chemical Theory and Computation **11**, 4077 (2015).
[69] G. Li Manni, R. K. Carlson, S. Luo, D. Ma, J. Olsen, D. G. Truhlar, and L. Gagliardi, Journal of Chemical Theory and Computation **10**, 3669 (2014).
[70] L. Gagliardi, D. G. Truhlar, G. Li Manni, R. K. Carlson, C. E. Hoyer, and J. L. Bao, Accounts of Chemical Research **50**, 66 (2017).
[71] R. Pandharkar, M. R. Hermes, D. G. Truhlar, and L. Gagliardi, The Journal of Physical Chemistry Letters **11**, 10158 (2020).
[72] A. O. Mitrushenkov, G. Fano, F. Ortolani, R. Linguerri, and P. Palmieri, The Journal of Chemical Physics **115**, 6815 (2001).
[73] G. K.-L. Chan and M. Head-Gordon, The Journal of Chemical Physics **116**, 4462 (2002).
[74] S. Guo, M. A. Watson, W. Hu, Q. Sun, and G. K.-L. Chan, Journal of Chemical Theory and Computation **12**, 1583 (2016).
[75] J. M. Bofill and P. Pulay, The Journal of Chemical Physics **90**, 3637 (1989).
[76] E. R. Sayfutyarova, Q. Sun, G. K.-L. Chan, and G. Knizia, Journal of Chemical Theory and Computation **13**, 4063 (2017).
[77] C. J. Stein and M. Reiher, CHIMIA **71**, 170 (2017).
[78] A. Checa-Fernandez, A. Santos, A. Romero, and C. M. Dominguez, Catalysts **11**, 722 (2021).
[79] İ. Gulcin and S. H. Alwasel, Processes **10**, 132 (2022).
[80] P. Prete, A. Fiorentino, L. Rizzo, A. Proto, and R. Cucciniello, Current Opinion in Green and Sustainable Chemistry **28**, 100451 (2021).
[81] T. A. Sales, I. G. Prandi, A. A. de Castro, D. H. Leal, E. F. da Cunha, K. Kuca, and T. C. Ramalho, International Journal of Molecular Sciences **20**, 1829 (2019).
[82] A. Eivazihollagh, I. Svanedal, H. Edlund, and M. Norgren, Journal of Molecular Liquids **278**, 688 (2019).
[83] I. S. S. Pinto, I. F. F. Neto, and H. M. Soares, Environmental Science and Pollution Research **21**, 11893 (2014).
[84] T. Egli, M. Bally, and T. Uetz, Biodegradation **1**, 121 (1990).
[85] H. A. Mottola, Toxicological & Environmental Chemistry **2**, 99 (1974).
[86] N. Hadrup, M. Frederiksen, E. B. Wedebye, N. G. Nikolov, T. K. Carøe, J. B. Sørli, K. B. Frydendall, B. Liguori, C. S. Sejbaek, P. Wolkoff, *et al.*, Journal of Applied Toxicology **42**, 130 (2022).
[87] R. S. Dybczyński, Z. Samczyński, and E. Chajduk, Critical Reviews in Analytical Chemistry , 1 (2021).
[88] A. D. Becke, Phys. Rev. A **38**, 3098 (1988).
[89] S. Grimme, J. Antony, S. Ehrlich, and H. Krieg, The Journal of Chemical Physics **132** (2010).
[90] S. Grimme, S. Ehrlich, and L. Goerigk, Journal of Computational Chemistry **32**, 1456 (2011).
[91] A. D. Becke and E. R. Johnson, The Journal of Chemical Physics **123** (2005).
[92] E. R. Johnson and A. D. Becke, The Journal of Chemical Physics **123** (2005).
[93] E. R. Johnson and A. D. Becke, The Journal of Chemical Physics **124** (2006).
[94] F. Weigend, F. Furche, and R. Ahlrichs, J. Chem. Phys. **119**, 12753 (2003).
[95] F. Weigend and R. Ahlrichs, Phys. Chem. Chem. Phys. **7**, 3297 (2005).
[96] F. Weigend, Phys. Chem. Chem. Phys. **8**, 1057 (2006).
[97] A. Klamt and G. Schüürmann, J. Chem. Soc., Perkin Trans. 2 , 799 (1993).
[98] R. Ahlrichs, M. Bär, M. Häser, H. Horn, and C. Kölmel, Chemical Physics Letters **162**, 165 (1989).
[99] O. Treutler and R. Ahlrichs, The Journal of Chemical Physics **102**, 346 (1995).
[100] F. Furche, R. Ahlrichs, C. Hättig, W. Klopper, M. Sierka, and F. Weigend, WIREs Computational Molecular Science **4**, 91 (2014).
[101] Quriosity, `http://www.basf.com/supercomputer` (2023), accessed: 2023-10-30.
[102] L. Helm and A. E. Merbach, Chemical Reviews **105**, 1923 (2005).

[103] T. K. Sham, J. B. Hastings, and M. L. Perlman, Journal of the American Chemical Society **102**, 5904 (1980).
[104] M. Grant and R. B. Jordan, Inorganic Chemistry **20**, 55 (1981).
[105] B. Kallies and R. Meier, Inorganic Chemistry **40**, 3101 (2001).
[106] J. P. Perdew, K. Burke, and M. Ernzerhof, Phys. Rev. Lett. **77**, 3865 (1996).
[107] J. Tao, J. P. Perdew, V. N. Staroverov, and G. E. Scuseria, Phys. Rev. Lett. **91**, 146401 (2003).
[108] J. W. Furness, A. D. Kaplan, J. Ning, J. P. Perdew, and J. Sun, The Journal of Physical Chemistry Letters **11**, 8208 (2020).
[109] V. N. Staroverov, G. E. Scuseria, J. Tao, and J. P. Perdew, The Journal of Chemical Physics **119**, 12129 (2003).
[110] A. D. Becke, The Journal of Chemical Physics **98**, 5648 (1993).
[111] C. Adamo and V. Barone, The Journal of Chemical Physics **110**, 6158 (1999).
[112] Y. Zhao and D. G. Truhlar, Theoretical Chemistry Accounts **120**, 215 (2008).
[113] S. Grimme, A. Hansen, S. Ehlert, and J.-M. Mewes, The Journal of Chemical Physics **154** (2021).
[114] O. A. Vydrov and T. Van Voorhis, The Journal of Chemical Physics **133** (2010).
[115] Q. Sun, J. Yang, and G. K.-L. Chan, Chemical Physics Letters **683**, 291 (2017).
[116] Q. Sun, T. C. Berkelbach, N. S. Blunt, G. H. Booth, S. Guo, Z. Li, J. Liu, J. D. McClain, E. R. Sayfutyarova, S. Sharma, *et al.*, Wiley Interdisciplinary Reviews: Computational Molecular Science **8**, e1340 (2018).
[117] J. Kirkpatrick, B. McMorrow, D. H. P. Turban, A. L. Gaunt, J. S. Spencer, A. G. D. G. Matthews, A. Obika, L. Thiry, M. Fortunato, D. Pfau, L. R. Castellanos, S. Petersen, A. W. R. Nelson, P. Kohli, P. Mori-Sánchez, D. Hassabis, and A. J. Cohen, DM21 Pyscf interface, `https://github.com/google-deepmind/deepmind-research/tree/master/density_functional_approximation_dm21` (2021).
[118] E. Edler and M. Stein, European Journal of Inorganic Chemistry **2014**, 3587 (2014).
[119] H. Eshuis, J. Yarkony, and F. Furche, The Journal of Chemical Physics **132**, 234114 (2010).
[120] H. Eshuis, J. E. Bates, and F. Furche, Theoretical Chemistry Accounts **131**, 1084 (2012).
[121] J. E. Bates and F. Furche, The Journal of Chemical Physics **139** (2013).
[122] C. Hättig and F. Weigend, The Journal of Chemical Physics **113**, 5154 (2000).
[123] F. Weigend, A. Köhn, and C. Hättig, The Journal of Chemical Physics **116**, 3175 (2002).
[124] F. Neese, F. Wennmohs, U. Becker, and C. Riplinger, The Journal of Chemical Physics **152**, 224108 (2020).
[125] F. Weigend, M. Häser, H. Patzelt, and R. Ahlrichs, Chemical physics letters **294**, 143 (1998).
[126] C. Hättig, Physical Chemistry Chemical Physics **7**, 59 (2005).
[127] F. Neese, *ORCA user manual*, FAccTs GmbH (2022), login required.
[128] Z. Fang, Z. Lee, K. A. Peterson, and D. A. Dixon, Journal of Chemical Theory and Computation **12**, 3583 (2016).
[129] L. W. Bertels, J. Lee, and M. Head-Gordon, Journal of Chemical Theory and Computation **17**, 742 (2021).
[130] F. Haase and R. Ahlrichs, Journal of Computational Chemistry **14**, 907 (1993).
[131] S. Grimme, The Journal of Chemical Physics **118**, 9095 (2003).
[132] F. D. Malone, A. Mahajan, J. S. Spencer, and J. Lee, Journal of Chemical Theory and Computation **19**, 109 (2023).
[133] J. Dunning, Thom H., The Journal of Chemical Physics **90**, 1007 (1989).
[134] G. K.-L. Chan, The Journal of Chemical Physics **120**, 3172 (2004).
[135] D. Ghosh, J. Hachmann, T. Yanai, and G. K.-L. Chan, The Journal of Chemical Physics **128** (2008).
[136] S. Sharma and G. K.-L. Chan, The Journal of Chemical Physics **136** (2012).
[137] S. Sharma and G. K.-L. Chan, Stackblock, `https://github.com/sanshar/StackBlock` (2020).
[138] A. Khedkar and M. Roemelt, Journal of Chemical Theory and Computation **15**, 3522 (2019).
[139] C. J. Stein and M. Reiher, Journal of Chemical Theory and Computation **12**, 1760 (2016).
[140] C. J. Stein and M. Reiher, Journal of Computational Chemistry (2019).
[141] V. Veryazov, P. Å. Malmqvist, and B. O. Roos, International Journal of Quantum Chemistry **111**, 3329 (2011).
[142] P. Pulay and T. P. Hamilton, The Journal of Chemical Physics **88**, 4926 (1988).
[143] Z. Tóth and P. Pulay, Journal of Chemical Theory and Computation **16**, 7328 (2020).
[144] D. S. King and L. Gagliardi, Journal of Chemical Theory and Computation **17**, 2817 (2021).
[145] Y. Ma and H. Ma, The Journal of Chemical Physics **138** (2013).
[146] R. S. Mulliken, The Journal of chemical physics **23**, 1833 (1955).
[147] J. Pipek and P. G. Mezey, The Journal of Chemical Physics **90**, 4916 (1989).
[148] P.-O. Widmark, P.-A. Malmqvist, and B. O. Roos, Theoretica chimica acta **77**, 291 (1990).
[149] B. O. Roos, R. Lindh, P.-A. Malmqvist, V. Veryazov, and P.-O. Widmark, The Journal of Physical Chemistry A **108**, 2851 (2004).
[150] B. O. Roos, R. Lindh, P.-A. Malmqvist, V. Veryazov, and P.-O. Widmark, The Journal of Physical Chemistry A **109**, 6575 (2005).
[151] P. Pinski and F. Eich, ActiveSpaceFinder, `https://github.com/HQSquantumsimulations/ActiveSpaceFinder` (2022), accessed: 2023-06-20.
[152] A. Klamt, The Journal of Physical Chemistry **99**, 2224 (1995).
[153] A. Klamt, V. Jonas, T. Bürger, and J. C. W. Lohrenz, The Journal of Physical Chemistry A **102**, 5074 (1998).
[154] A. Klamt, F. Eckert, and M. Hornig, Journal of Computer-Aided Molecular Design **15**, 355 (2001).
[155] BIOVIA COSMOtherm, Version C30, Release 18, `https://www.3ds.com/products-services/biovia/products/molecular-modeling-simulation/solvation-chemistry/biovia-cosmotherm/` (2018), accessed: 2023-06-20.
[156] F. Eckert and A. Klamt, AIChE Journal **48**, 369 (2002).
[157] D. Rappoport and F. Furche, The Journal of chemical physics **133** (2010).

[158] B. J. Coe and S. J. Glenwright, Coordination Chemistry Reviews **203**, 5 (2000).
[159] T. J. Lee and P. R. Taylor, International Journal of Quantum Chemistry **36**, 199 (1989).
[160] C. L. Janssen and I. M. B. Nielsen, Chemical Physics Letters **290**, 423 (1998).
[161] C. Mejuto-Zaera, D. Tzeli, D. Williams-Young, N. M. Tubman, M. Matoušek, J. Brabec, L. Veis, S. S. Xantheas, and W. A. de Jong, Journal of Chemical Theory and Computation **18**, 687 (2022).
[162] G. P. Chen, V. K. Voora, M. M. Agee, S. G. Balasubramani, and F. Furche, Annual Review of Physical Chemistry **68**, 421 (2017).
[163] J. Lee, H. Q. Pham, and D. R. Reichman, Journal of Chemical Theory and Computation **18**, 7024 (2022).
[164] M. Bensberg and M. Reiher, The Journal of Physical Chemistry Letters **14**, 2112 (2023).
[165] C. J. Cramer and D. G. Truhlar, Phys. Chem. Chem. Phys. **11**, 10757 (2009).
[166] J. N. Harvey, in *Principles and Applications of Density Functional Theory in Inorganic Chemistry I* (Springer Berlin Heidelberg, Berlin, Heidelberg, 2004) pp. 151–184.
[167] M. Swart and M. Gruden, Accounts of Chemical Research **49**, 2690 (2016).
[168] A. Klamt and M. Diedenhofen, The Journal of Physical Chemistry A **119**, 5439 (2015).

Appendix A: Complete Basis Set Extrapolation

To get an estimation for the single-point energy in the complete basis set (CBS) limit, we performed a two-point CBS extrapolation for the DLPNO-CCSD(T) calculations using the def2-TZVPP and def2-QZVPP basis sets, and also for the AFQMC calculations using the def2-SVP and def2-TZVP basis sets. As described in section 8.1.3.5 of the `ORCA` manual, [127] the SCF energy in the CBS limit is given by

$$E_{\mathrm{SCF}}^{(\infty)} = E_{\mathrm{SCF}}^{(X)} - \frac{E_{\mathrm{SCF}}^{(X)} - E_{\mathrm{SCF}}^{(Y)}}{\exp(-\alpha\sqrt{X}) - \exp(-\alpha\sqrt{Y})} * \exp(\alpha\sqrt{X}) \tag{A1}$$

with X, Y = 3, 4 (2, 3 for AFQMC) being the cardinal numbers of the basis sets and $\alpha = 7.88$ for a (3,4) and $\alpha = 10.39$ for a (2,3) extrapolation for the "def2" basis sets. The extrapolated correlation energy is given by

$$E_{\mathrm{corr}}^{(\infty)} = \frac{X^{\beta} E_{\mathrm{corr}}^{(X)} - Y^{\beta} E_{\mathrm{corr}}^{(Y)}}{X^{\beta} - Y^{\beta}} \tag{A2}$$

with $\beta = 2.97$ for the (3,4) and $\beta = 2.40$ for the (2,3) extrapolation.

Appendix B: Spin Contamination in DFT for the Spin-State Energetics of Fe(III)-NTA

Figure 17 shows how the spin contamination, $\langle \hat{S}^2 \rangle - \langle \hat{S}^2 \rangle_{\mathrm{theo}}$, increases with an increasing amount of HF exchange in a hybrid DFT functional in case of the IS and LS states of Fe(III)-NTA. For the HS state, the relationship is roughly an order of magnitude weaker: while $\langle \hat{S}^2 \rangle - \langle \hat{S}^2 \rangle_{\mathrm{theo}}$ also increases with an increasing amount of HF exchange, the difference, i.e. spin contamination, at 60% HF exchange amounts to only 0.012.

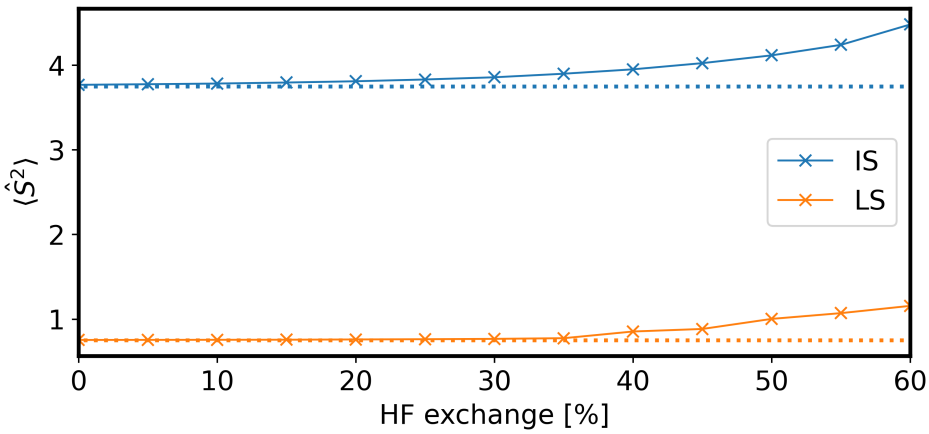

FIG. 17. Influence of the amount of HF exchange in DFT on the computed $\langle \hat{S}^2 \rangle$ in an unrestricted Kohn-Sham formalism for the IS and LS states of Fe(III)-NTA. The amount of HF exchange in the hybrid functional B3LYP was varied between 0 and 60% in steps of 5%. The basis sets used are def2-QZVPP. The dotted lines indicate the theoretical $\langle \hat{S}^2 \rangle$ without any spin contamination, i.e. $\langle \hat{S}^2 \rangle_{\mathrm{theo}}$.

Appendix C: Energies of Reactions with Varying Amounts of Explicit Water Molecules

In order to apply multi-reference active space methods to the calculation of reaction energies with different amounts of explicit water molecules coordinating to the TM-NTA complexes on reactant and product side, we balanced the stoichiometry by placing the additional water molecule (which would normally be calculated within a separate calculation) at 100 Å distance from the closest ligand atom of the TM-NTA complex. It was verified that the residual interaction between the additional water molecule and the remainder leads to errors of below 0.1 kJ/mol in the respective CASSCF energy. This workaround was required to ensure that, within the on-top methods NEVPT2 and MC-PDFT, the water molecule was handled at exactly the same level of theory as the inactive space of the remainder, for the simple reason that the implementations which we employed require non-empty active spaces thus not directly allowing a calculation of a completely inactive individual water molecule.

Appendix D: Geometrical Structure of Fe(III)-hexaaqua

As described in section III B 6 b in the main text, the results obtained with some electronic-structure methods, in particular NEVPT2 (3d4d), are significantly less accurate for the reactions involving Fe(III) than their respective results for all other reactions. In Figure 18 it can be seen that the optimized structures at the BP86-D3(BJ)/def2-QZVP level using COSMO with $\epsilon = 78$, see section II A in the main text, are qualitatively different between Fe(III)-hexaaqua and all hexaaqua complexes involving dicationic TM centers (Mn(II)-hexaaqua being representatively shown), due to a different orientation of the water molecules. The water molecules orientate themselves such that the hydrogen atoms are facing almost exactly away from the Fe(III) ion, while they align at an angle for the other (dicationic) TM ions. This does not seem to be due to the functional used, as qualitatively very similar structures are obtained when B3LYP is used instead of BP86 for the structure optimization. The angles drawn are approximately 90° (larger than 86.9°) in case of Fe(III)-hexaaqua, while they range between 33° and 60° in case of all other hexaaqua complexes.

As this could in principle be an artifact from the use of the continuum solvation model COSMO to represent the solvent, we re-optimized the structures using Direct-COSMO-RS (DCOSMO-RS) instead, which is based on explicit solvent molecules. [168] However, a major downside of this approach is a more difficult convergence behavior and a higher likelihood to arrive at saddle-point structures having vibrational modes with imaginary frequencies. All resulting structures, including Fe(III)-hexaaqua, indeed had similar symmetries with the above-mentioned angles for Fe(III)-hexaaqua now being around 49°. However, repeating the NEVPT2 (3d4d) single-point calculations with these structures even led to an increase in errors with respect to the experimental values for the reactions involving Fe(III). We therefore conclude that the shortcomings of the COSMO solvation model are not the main reason for the outlier behavior of reactions involving Fe(III).

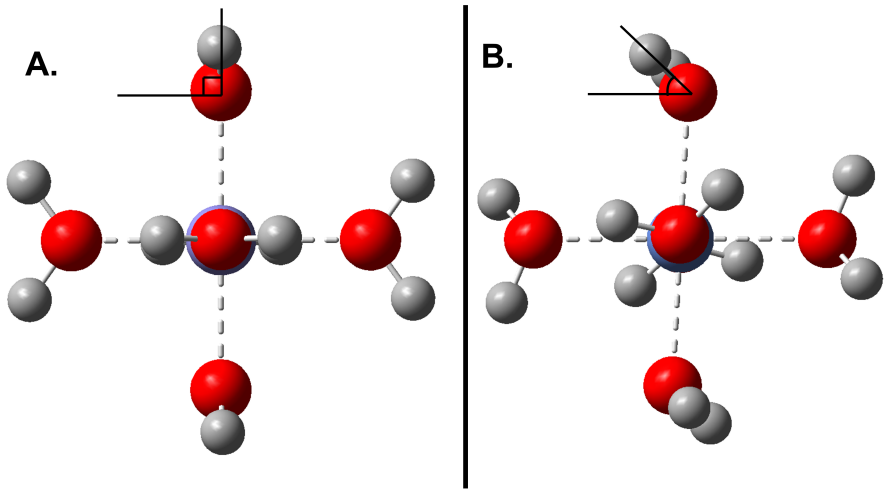

FIG. 18. Optimized structures of at the BP86-D3(BJ)/def2-QZVP level using COSMO with $\epsilon = 78$ of **A.** Fe(III)-hexaaqua and **B.** Mn(II)-hexaaqua. For further information see section II A in the main text.

Appendix E: Additional Figures and Tables

Method/Basis	ΔG^0 [kJ/mol]	
	IS - HS	**LS - HS**
BP86	20.3	-1.8
PBE	24.0	-1.2
TPSS	17.3	-20.8
r^2SCAN	68.4	40.7
r^2SCAN-3c	67.6	45.0
M06-L	95.2	93.6
TPSSh	36.1	11.0
B3LYP	58.6	52.2
PBE0	71.9	76.1
M06-2X	122.7	166.5
ωB97M-V	59.2	33.7
DM21	/	-49.1
UHF	281.8	377.5
ROHF	289.6	392.9
RPA	47.8	16.5
RPA-AXK	59.7	36.8
U-MP2	111.9	164.6
RO-MP2	121.7	111.1
U-CCSD(T)/def2-TZVP	105.3	109.6
RO-CCSD(T)/def2-SVP	116.8	122.0
RO-CCSD(T)/def2-TZVP	104.9	106.6
RO-CCSD(T)/(2,3)CBS	102.4	101.3
U-DLPNO-CCSD(T)/def2-TZVP	123.8	132.8
RO-DLPNO-CCSD(T)/def2-TZVP	125.2	132.8
RO-DLPNO-CCSD(T)/def2-TZVPP	110.2	112.8
RO-DLPNO-CCSD(T)/def2-QZVPP	111.0	106.3
RO-DLPNO-CCSD(T)/(3,4)CBS	108.9	97.7
AFQMC/def2-SVP (ROHF trial)	157.0 ± 1.3	145.4 ± 1.3
AFQMC/def2-TZVP (ROHF trial)	147.2 ± 1.3	138.8 ± 1.4
AFQMC/(2,3)CBS (ROHF trial)	146.0 ± 2.2	138.9 ± 2.4
AFQMC/def2-TZVP ((5,5)CASSCF trial)	144.1 ± 1.4	131.4 ± 1.6
(5,5)CASSCF	260.9	349.4
(5,5)ftPBE	-39.4	-39.4
(5,5)tPBE	-9.2	23.6
(5,5)ftPBE0	35.7	57.8
(5,5)tPBE0	58.4	105.0
(5,5)NEVPT2	49.3	43.4
(9,12)CASSCF	153.7	176.6
(9,12)ftPBE	-34.5	-68.0
(9,12)tPBE	-13.7	-22.2
(9,12)ftPBE0	12.6	-6.8
(9,12)tPBE0	28.1	27.5
(9,12)NEVPT2	57.6	41.7
(17,20)DMRG-CASSCF	114.5	74.0
(17,20)DMRG-NEVPT2	117.7	127.4
(49,36)DMRG-CASCI	99.2	85.2
(49,36)DMRG-NEVPT2 (NEVPT2 MBD = 400)	125.6	114.3
(49,36)DMRG-NEVPT2 (NEVPT2 MBD = 600)	124.3	113.2
(49,36)DMRG-CASCI$_{\text{AVAS}}$	118.1	74.8
(49,36)DMRG-NEVPT2$_{\text{AVAS}}$ (NEVPT2 MBD = 400)	108.0	106.5
(49,36)DMRG-NEVPT2$_{\text{AVAS}}$ (NEVPT2 MBD = 600)	107.1	105.3

TABLE IV. Spin-state energetics of Fe(III)-NTA for all investigated electronic-structure methods. If not indicated otherwise, the basis sets used are def2-QZVPP. The differences in Gibbs free energies, ΔG^0, between the IS and HS as well as the LS and HS states are shown. The prefixes "RO-" and "U-" refer to the use of restricted open-shell Hartree-Fock (ROHF) and unrestricted Hartree-Fock (UHF) molecular orbitals, respectively. MBD refers to the maximum bond dimension within DMRG calculations, which is 1000 unless indicated otherwise. For further information see section II and section III A in the main text.

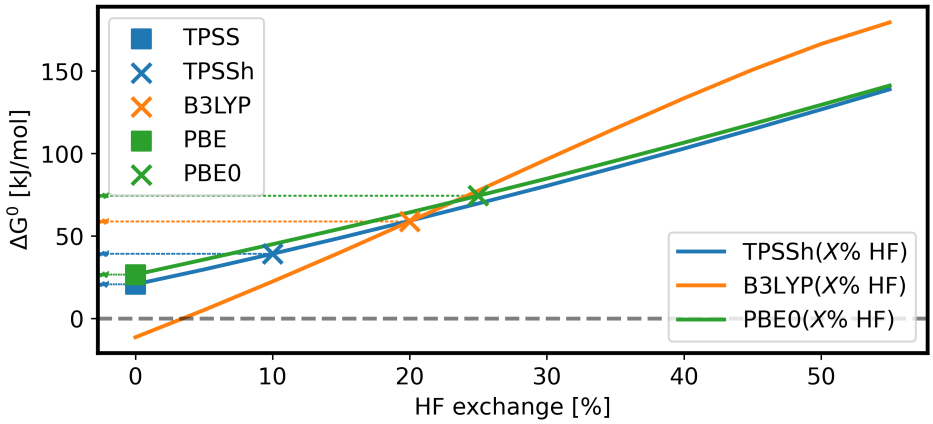

FIG. 19. Influence of the amount of HF exchange in DFT on the energy gap, ΔG^0, between the IS and HS state of Fe(III)-NTA. The basis sets used are def2-QZVPP. For further information see Figure 3 in the main text.

TM Ion	$\mathbf{\Delta_r G^0}$ [kJ/mol]	**Explicit $\mathbf{H_2O}$**
Fe(III)	-22.9	2
Mn(II)	-4.5	2
Fe(II)	-11.4	2
Co(II)	7.4	1
Ni(II)	-31.5	2
Cu(II)	N/A	1

TABLE V. Computed Gibbs free energies, $\Delta_r G^0$, for the addition of a second explicit water molecule to the TM-NTA complexes, see Equation 2 in the main text, at the B3LYP-D3(BJ)/def2-TZVP level. No stable structure was found for $[CuNTA(H_2O)_2]^-$.

TM Ion	**# Unpaired Electrons**	**Aqua Complex**		**NTA Complex**	
		BP86	**B3LYP**	**BP86**	**B3LYP**
Fe(III)	5	-1722.45575	-1721.95003	-2155.93412	-2155.15205
	3	-1722.43366	-1721.91509	-2155.92652	-2155.13213
	1	-1722.43945	-1721.91357	-2155.93124	-2155.13448
Mn(II)	5	-1609.96841	-1609.49502	-2043.37508	-2042.62909
	3	-1609.91895	-1609.43655	-2043.34652	-2042.57434
	1	-1609.90649	-1609.42109	-2043.32646	-2042.56216
Fe(II)	4	-1722.68248	-1722.18398	-2156.09328	-2155.32238
	2	-1722.65285	-1722.14639	-2156.09160	-2155.29862
	0	-1722.65764	-1722.14772	-2156.07789	-2155.28956
Co(II)	3	-1841.76156	-1841.23914	-2198.68769	-2197.93023
	1	-1841.74547	-1841.21314	-2198.67789	-2197.90390
Ni(II)	2	-1967.33999	-1966.79234	-2400.75476	-2399.93218
	0	-1967.31846	-1966.76563	-2400.74792	-2399.90781
Cu(II)	1	-2099.49914	-2098.92847	-2456.43390	-2455.62675

TABLE VI. Absolute energies in Hartree for the optimized structure of each spin state for all studied compounds using BP86-D3(BJ) and B3LYP-D3(BJ) in combination with the def2-QZVP basis sets and COSMO with $\epsilon = 78$.

M_1/M_2	RO-CCSD(T)	U-CCSD(T)
Fe(III)/Cu(II)	19.4	19.0
Fe(III)/Ni(II)	37.1	36.7
Fe(III)/Co(II)	49.3	49.0
Fe(III)/Fe(II)	52.5	52.2
Fe(III)/Mn(II)	64.7	64.2
Cu(II)/Ni(II)	17.7	17.7
Cu(II)/Co(II)	29.9	30.0
Cu(II)/Fe(II)	33.0	33.2
Cu(II)/Mn(II)	45.3	45.2
Ni(II)/Co(II)	12.2	12.3
Ni(II)/Fe(II)	15.4	15.5
Ni(II)/Mn(II)	27.6	27.5
Co(II)/Fe(II)	3.1	3.2
Co(II)/Mn(II)	15.4	15.3
Fe(II)/Mn(II)	12.2	12.1

TABLE VII. Computed Gibbs free energies, $\Delta_r G^0$, in kJ/mol using CCSD(T) in combination with restricted open-shell Hartree-Fock (ROHF) and unrestricted Hartree-Fock (UHF) molecular orbitals for the selectivity of NTA. The basis sets used are def2-TZVP.

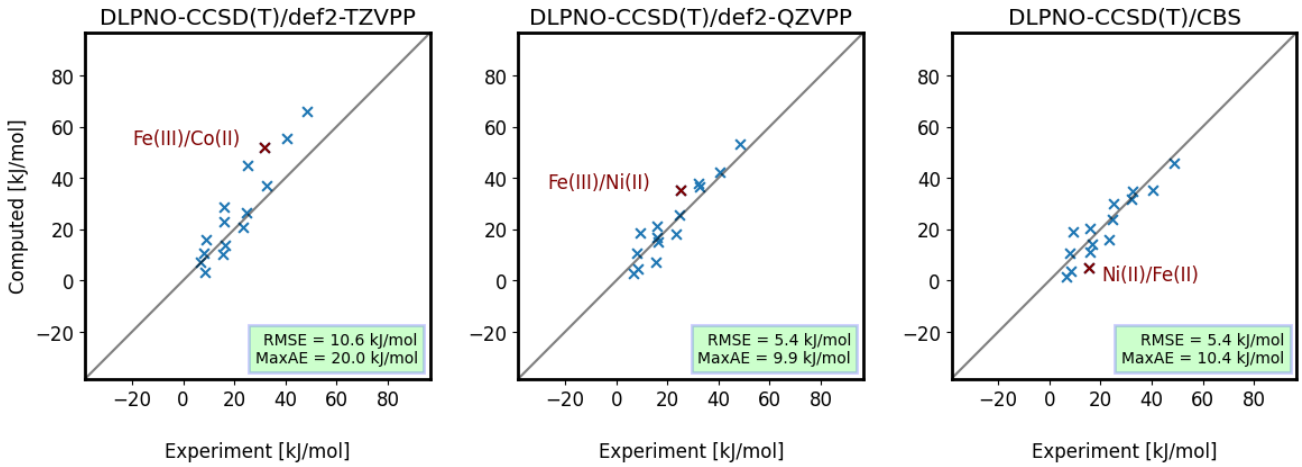

FIG. 20. Computed Gibbs free energies, $\Delta_r G^0$, using DLPNO-CCSD(T) for the selectivity of NTA with respect to six different TM ions, plotted against the respective experimental values. The results using def2-TZVPP and def2-QZVPP basis sets are shown along with the results of the (3,4)CBS extrapolation. For further information see Figure 11 in the main text.

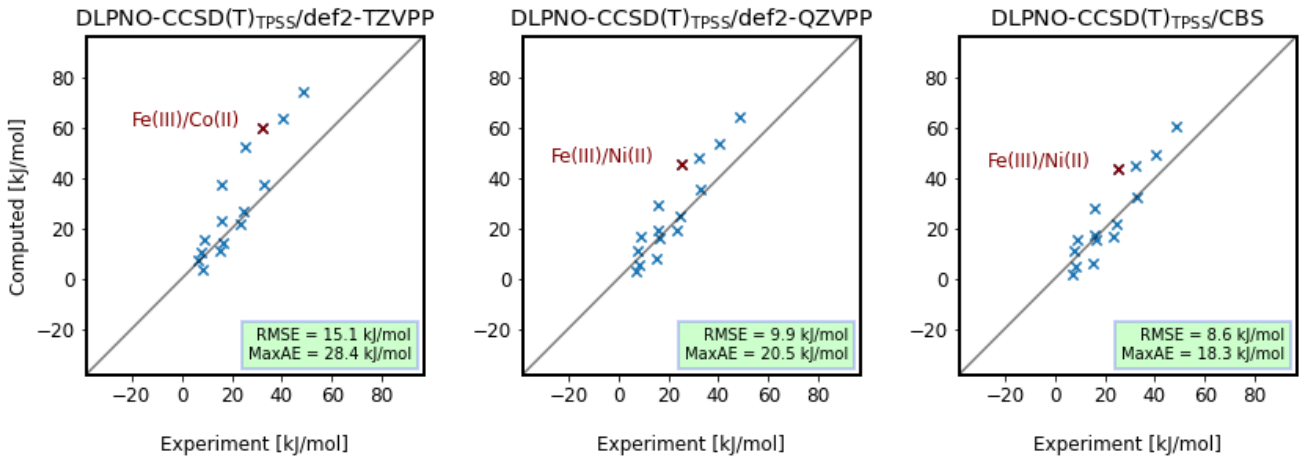

FIG. 21. Computed Gibbs free energies, $\Delta_r G^0$, using DLPNO-CCSD(T)$_{\mathrm{TPSS}}$ for the selectivity of NTA with respect to six different TM ions, plotted against the respective experimental values. The results using def2-TZVPP and def2-QZVPP basis sets are shown along with the results of the (3,4)CBS extrapolation. For further information see Figure 11 in the main text.

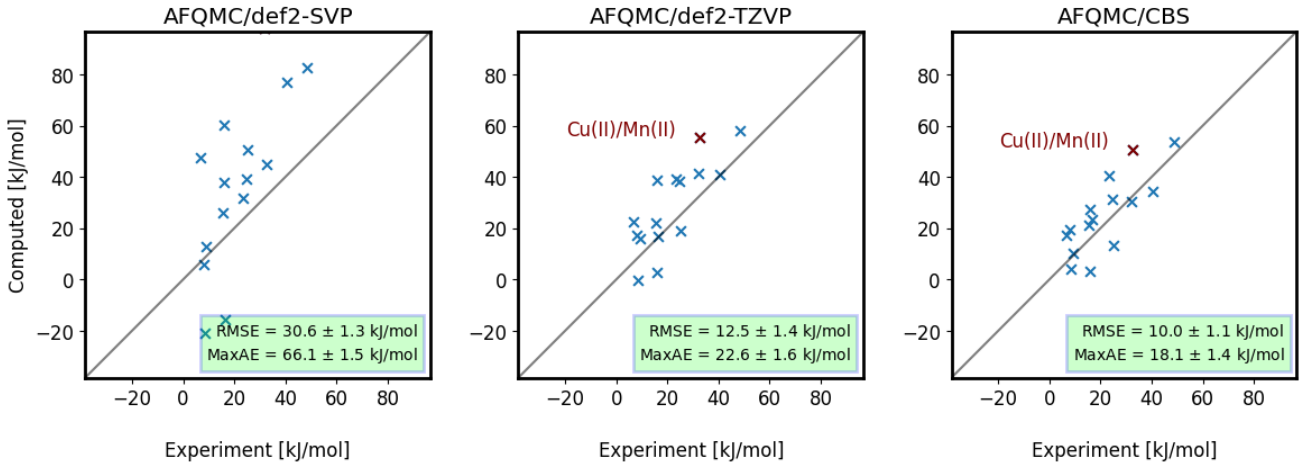

FIG. 22. Computed Gibbs free energies, $\Delta_r G^0$, using AFQMC for the selectivity of NTA with respect to six different TM ions, plotted against the respective experimental values. The results using def2-SVP and def2-TZVP basis sets are shown along with the results of the (2,3)CBS extrapolation. For further information see Figure 12 in the main text.

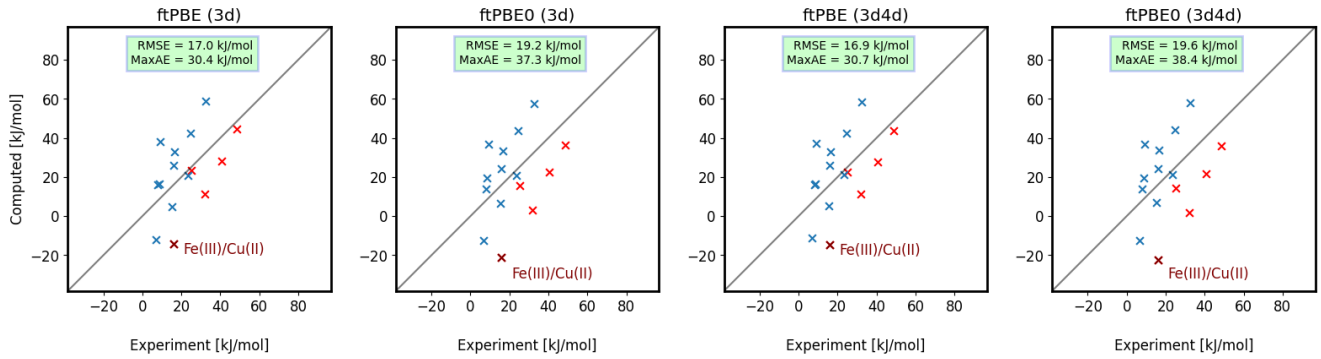

FIG. 23. Computed Gibbs free energies, $\Delta_r G^0$, using the active space method MC-PDFT in combination with the ftPBE and ftPBE0 density functionals for the selectivity of NTA with respect to six different TM ions, plotted against the respective experimental values. The results using the "3d" and "3d4d" active spaces are shown. The basis sets used are def2-QZVPP. For further information see Figure 13 in the main text.

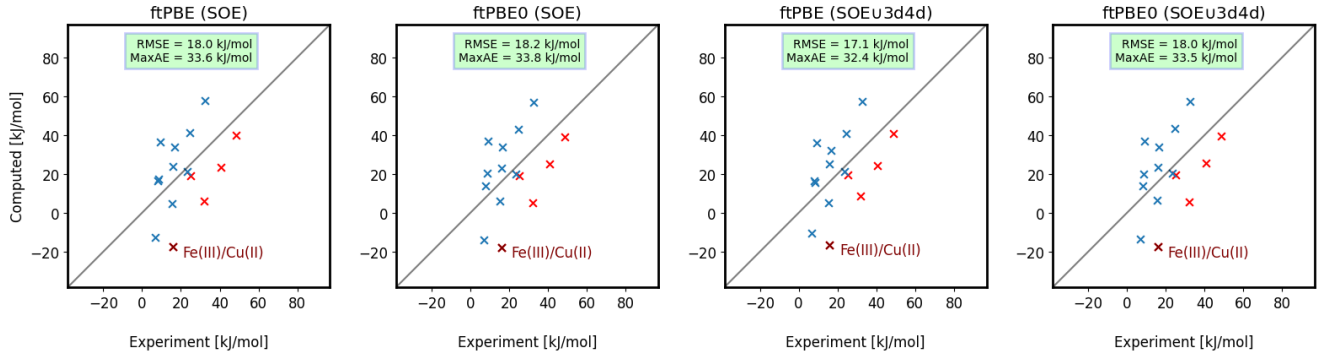

FIG. 24. Computed Gibbs free energies, $\Delta_r G^0$, using the active space method MC-PDFT in combination with the ftPBE and ftPBE0 density functionals for the selectivity of NTA with respect to six different TM ions, plotted against the respective experimental values. The results using the "SOE" and "SOE∪3d4d" active spaces are shown. The basis sets used are def2-QZVPP. For further information see Figure 15 in the main text.

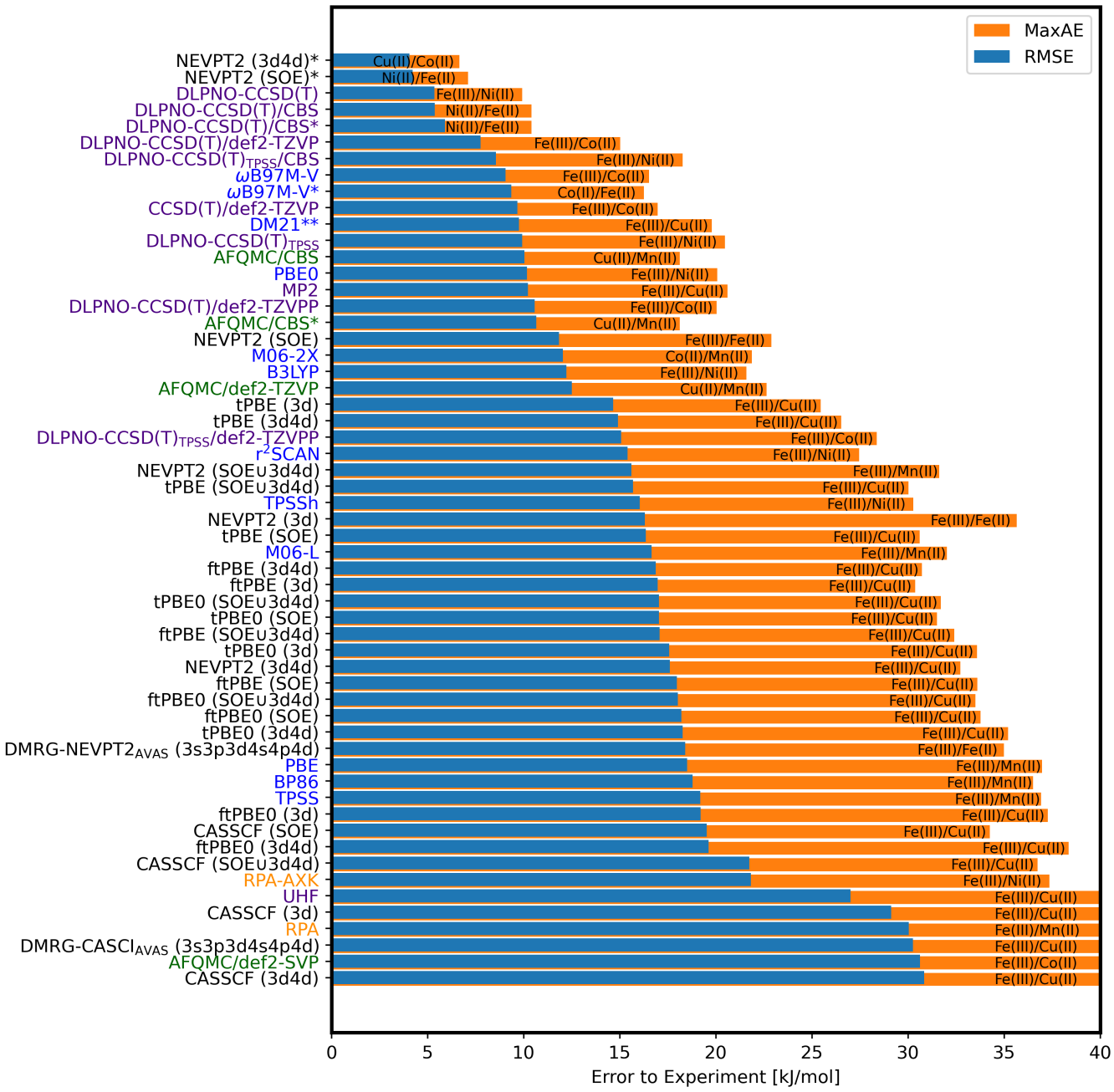

FIG. 25. Root mean square error (RMSE) and maximum absolute error (MaxAE) of the computed Gibbs free energies for the selectivity of NTA with respect to experimental values for all investigated electronic-structure methods. If not indicated otherwise, the basis sets used are def2-QZVPP. The two TM ions involved in the reaction causing the MaxAE are shown for each method. The methods are categorized according to the structure of the Computational Details section, section II in the main text, which is indicated by the different colors. The asterisk indicates that the reactions involving Fe(III) were excluded from the statistics which is shown for NEVPT2 (3d4d) and NEVPT2 (SOE), as well as for the most accurate method of other categories. For DM21 the reactions involving Mn(II) are missing due to non-convergence. As the horizontal axis is cut off, the MaxAEs of the bottom six methods are, in order: 54.3, 58.0, 56.3, 60.2, 66.1 and 61.2 kJ/mol.

Appendix F: Molecular Structures

The following structures were optimized at the BP86-D3(BJ)/def2-QZVP level using COSMO with $\epsilon = 78$.

[Fe NTA $(H_2O)_2$] (HS)

C	-1.5889369	-0.8528778	-1.8732487
C	-2.1952207	-0.9276224	0.5083579
C	-0.3692881	-2.3486012	-0.3245008
O	-0.6760450	0.0989312	-3.8826536
O	-1.3079982	1.2957057	0.6482661
O	1.0802469	-3.1877678	1.4118367
O	0.2992480	0.6362684	-1.9387585
O	-3.4130738	0.9726350	1.3492347
C	-0.5951599	0.0010950	-2.6609172
C	-2.3647330	0.5515026	0.8624209
C	0.6227827	-2.2068279	0.8324041
N	-1.1327132	-1.1026736	-0.4953382
Fe	0.3902284	0.5174551	-0.0027221
O	2.5783470	0.6597988	-0.5270423
H	-2.5302947	-0.2889401	-1.8445216
H	-1.7888211	-1.7886589	-2.4105833
H	-1.9056894	-1.4443936	1.4334919
H	-3.1482157	-1.3552934	0.1723903
H	0.2177929	-2.5357656	-1.2341807
H	-1.0235509	-3.2155365	-0.1633923
H	2.6884158	0.5351241	-1.4857889
H	3.1221628	-0.0285429	-0.1066529
O	0.9589813	-0.9668898	1.1160630
O	1.0976602	2.2042886	1.0651240
H	1.8945526	2.6301760	0.7045097
H	0.4392189	2.9033636	1.2213048

[Fe NTA $(H_2O)_2$] (IS)

C	-1.0631696	-0.8986273	-1.9564065
C	-2.2726265	-0.8715147	0.2176117
C	-0.2213187	-2.2369457	0.0042160
O	-1.3060002	0.9464995	-3.4925138
O	-1.4204678	1.2219942	1.0540575
O	0.8952750	-2.7897046	2.0745880
O	-0.2503233	1.3405105	-1.5583148
O	-3.5805554	0.7176234	1.4194742
C	-0.9043439	0.5588651	-2.4011021
C	-2.4669757	0.4632095	0.9502270
C	0.5498120	-1.9156119	1.2884213
N	-0.9483701	-1.0225278	-0.4731344
Fe	0.2137470	0.5250676	0.0955542
O	1.9886683	-0.4000745	-1.1969343
H	-2.0097221	-1.3160535	-2.3146150
H	-0.2431632	-1.4604326	-2.4182724
H	-2.3697581	-1.6649618	0.9671875
H	-3.0803148	-1.0078491	-0.5091128
H	0.5200916	-2.5218690	-0.7507292
H	-0.9090669	-3.0759629	0.1513051
H	2.2755494	0.2246208	-1.8844300
H	2.7845954	-0.5673481	-0.6640381
O	0.8682823	-0.6398588	1.4466564
O	1.4404474	2.0311775	0.6137125
H	1.3158602	2.8791116	0.1523929
H	1.5437445	2.2366153	1.5593020

[Fe NTA $(H_2O)_2$] (LS)

C	-1.0290441	-0.9471117	-1.9865887
C	-2.2505436	-0.7922495	0.1582250
C	-0.2593185	-2.2544373	0.0162178
O	-1.3454085	0.8783278	-3.5342318
O	-1.1347371	1.1483476	1.0151618
O	0.8453748	-2.7999130	2.0922098
O	-0.2780587	1.3040005	-1.6070564
O	-3.2498211	0.8000765	1.6534429
C	-0.9188318	0.5115628	-2.4417824
C	-2.2565356	0.4618854	1.0159078
C	0.5342286	-1.9274094	1.2848894
N	-0.9221422	-1.0235290	-0.5013883
Fe	0.2526900	0.4497192	0.0039380
O	1.8221685	-0.2815654	-1.0936915
H	-1.9555949	-1.4065777	-2.3473606
H	-0.1824638	-1.4867161	-2.4264081
H	-2.5130292	-1.6526686	0.7833244
H	-3.0320380	-0.6959329	-0.6040366
H	0.4617231	-2.6044401	-0.7316186
H	-0.9840969	-3.0551564	0.1969690
H	2.1227503	0.3853924	-1.7373941
H	2.5891208	-0.4447721	-0.5150575
O	0.9052095	-0.6681693	1.3941789
O	1.4573655	1.9796179	0.5273073
H	1.0868407	2.8424014	0.2685815
H	1.5840897	2.0352695	1.4913642

$[Fe\,(H_2O)_6]^{3+}$

Fe	-1.9176571	0.9827915	-0.0431929
O	-0.4444516	0.4695124	-1.3153433
H	0.4920824	0.7234264	-1.2288059
O	-3.3930843	1.4940207	1.2267274
H	-4.3286711	1.2379372	1.1364616
O	-1.5992249	-0.7110159	0.9955371
H	-0.9406115	-1.3943048	0.7757491
O	-2.2348179	2.6767751	-1.0828449
H	-1.7330257	2.9679381	-1.8653284
O	-3.2576917	0.0255318	-1.2013460
H	-3.4972306	-0.9165258	-1.1371365
O	-0.5781522	1.9425546	1.1126021
H	-0.3416215	2.8851601	1.0453257
H	-0.5547938	-0.0310225	-2.1437574
H	-3.2871038	1.9943798	2.0558359
H	-2.0995833	-1.0037761	1.7783967
H	-2.8937551	3.3605984	-0.8655489
H	-3.7401014	0.4174101	-1.9515629
H	-0.0937950	1.5543888	1.8635118

$[Mn\,NTA\,(H_2O)_2]^{-}$

C	-1.8684658	-0.0672026	-1.4878994
C	0.2496725	-1.1743664	-2.0234222
C	0.1556322	1.2709085	-1.8684547
O	-1.8621173	0.5479025	0.8430121
O	0.3683450	-3.5326565	-1.5995919
O	2.2469873	2.4345738	-1.6954188
O	-3.7393022	0.9048311	-0.3442870
O	0.1262923	-2.1621146	0.1700347
C	-2.5561990	0.5273297	-0.2447483

C	0.2346632	-2.4016042	-1.0912426
C	1.4762946	1.6188201	-1.1529464
N	-0.4023319	-0.0082188	-1.4134495
Mn	0.1510226	-0.1214972	0.8207672
O	1.3090277	-1.1646259	2.4386844
H	-2.1748365	-1.1223096	-1.5271719
H	-2.2602237	0.4155084	-2.3958256
H	1.3076309	-0.9319910	-2.2004566
H	-0.1905132	-1.4397095	-2.9973340
H	-0.5545679	2.0713420	-1.6153310
H	0.3045409	1.3018796	-2.9592534
H	1.1811576	-2.1174719	2.2855603
H	1.0236335	-1.0017985	3.3532408
O	1.6736991	1.0645855	-0.0049578
O	-0.0052103	1.4286449	2.6037619
H	0.5747258	2.1938940	2.4527893
H	-0.8974816	1.7301165	2.3471804

$[Mn\,(H_2O)_6]^{2+}$

Mn	-1.9217173	0.9842118	-0.0407564
O	-0.3372295	0.2903132	-1.3719794
H	0.5432298	0.7008018	-1.3404575
O	-3.5045869	1.6757173	1.2898294
H	-4.3873834	1.2712600	1.2465926
O	-1.5164607	-0.7717972	1.1822254
H	-0.9630302	-1.4932022	0.8390635
O	-2.3114484	2.7357067	-1.2756943
H	-1.6571605	3.1294382	-1.8762020
O	-3.4676522	-0.0524174	-1.1767800
H	-3.5105851	-1.0192240	-1.2625855
O	-0.3758752	2.0223833	1.0941323
H	-0.3270697	2.9898779	1.1682538
H	-0.4818141	0.0394414	-2.2994066
H	-3.3633843	1.9092444	2.2223082
H	-2.1623226	-1.1883904	1.7764406
H	-2.8489311	3.4739148	-0.9429845
H	-3.7898744	0.3057896	-2.0209625
H	-0.0599944	1.6727109	1.9442428

$[Fe\,NTA\,(H_2O)_2]^{-}$

C	-2.0155331	2.0306045	-2.0674632
C	-4.2530465	1.9385644	-1.0848968
C	-3.1906192	-0.1456489	-1.8420172
O	-0.7501034	4.0331494	-1.6742089
O	-6.0346807	2.0810010	0.5008855
O	-3.6639581	-2.3546707	-1.0480009
O	-1.2667796	2.7598067	0.1063910
O	-3.9972719	1.5449839	1.2888999
C	-1.2936528	3.0409385	-1.1552956
C	-4.8212680	1.8279728	0.3436943
C	-3.1816684	-1.2426933	-0.7591939
N	-2.9857710	1.2156694	-1.3199647
Fe	-2.0765338	0.9895230	0.7081983
O	-1.2981255	0.9021126	2.7231076
H	-2.4719326	2.5629579	-2.9160343
H	-1.2385665	1.3691175	-2.4742871
H	-5.0242507	1.6294712	-1.8049699
H	-4.0779910	3.0118793	-1.2446726
H	-2.3680899	-0.3957105	-2.5252185
H	-4.1222652	-0.2224153	-2.4212371

H	-0.5195364	0.3231825	2.7901104
H	-1.8839300	0.6489920	3.4553685
O	-2.6197289	-0.9535525	0.3656969
O	0.0956872	0.0722261	0.3915584
H	-0.0270417	-0.7661387	-0.0838609
H	0.6835097	0.5999293	-0.1735985

$[Fe\,(H_2O)_6]^{2+}$

Fe	-1.9219853	0.9840921	-0.0432616
O	-0.4364704	0.2458699	-1.3784916
H	0.4965706	0.4645300	-1.2152278
O	-3.4038387	1.7250124	1.2923402
H	-4.3373055	1.5066175	1.1309029
O	-1.5610861	-0.6821838	1.2123991
H	-0.9153327	-1.3509966	0.9276775
O	-2.2732593	2.6466329	-1.3056916
H	-1.5418790	3.1169934	-1.7404216
O	-3.4325211	-0.1203880	-1.0737477
H	-3.2425906	-1.0123675	-1.4109859
O	-0.4102915	2.0850463	0.9903628
H	-0.5958798	2.9786138	1.3258139
H	-0.5491717	0.2791447	-2.3434236
H	-3.2880978	1.6864679	2.2567281
H	-2.2839591	-1.1744730	1.6370643
H	-2.9013325	3.3334464	-1.0240604
H	-3.9007330	0.3355849	-1.7940063
H	0.0558735	1.6281370	1.7113095

$[Co\,NTA\,H_2O]^{-}$

C	-0.0176436	1.4747909	-1.5040647
C	-1.8000263	-0.1838730	-1.1335888
C	0.4436088	-0.9240969	-1.8257196
O	1.8021311	2.9994379	-1.1334937
O	-3.7002370	0.4259671	0.2062828
O	1.0629219	-3.2151986	-1.4449464
O	1.4247600	1.4278764	0.4278296
O	-1.6938287	0.3415311	1.2154795
C	1.1762987	2.0175977	-0.6993214
C	-2.4715589	0.2436105	0.1823785
C	0.7432137	-2.1333776	-0.9235762
N	-0.3558369	0.0938438	-1.1271512
Co	0.2270516	-0.0774497	0.9390357
O	0.9585668	-0.2369868	2.9236218
H	-0.8718098	2.1234971	-1.2647972
H	0.1776919	1.5782922	-2.5814611
H	-1.9486389	-1.2696633	-1.2182815
H	-2.3128652	0.2826510	-1.9870177
H	1.4160548	-0.4853234	-2.0903685
H	-0.0284909	-1.2594360	-2.7606661
H	0.4662797	-0.8264134	3.5198544
H	1.0236692	0.6066928	3.4026349
O	0.6849600	-1.9214621	0.3536785

$[Co\,(H_2O)_6]^{2+}$

Co	-1.9203194	0.9831784	-0.0429425
O	-0.3727376	0.2325396	-1.2565917
H	0.4252967	0.7869006	-1.3027105
O	-3.4668567	1.7357768	1.1696938
H	-4.2642046	1.1803484	1.2153723

O	-1.5781396	-0.6585890	1.1800306
H	-0.8675699	-1.2619477	0.9013976
O	-2.2592137	2.6229750	-1.2699980
H	-1.5227377	3.1702512	-1.5908988
O	-3.4731020	-0.0383059	-1.0405245
H	-3.3226329	-0.9560911	-1.3238313
O	-0.3675479	2.0055963	0.9538874
H	-0.5191798	2.9220953	1.2407332
H	-0.5654410	-0.0283496	-2.1731519
H	-3.2727944	1.9932374	2.0869497
H	-2.3076677	-1.2232423	1.4865477
H	-2.9543755	3.2427465	-0.9883932
H	-3.8516911	0.4131495	-1.8147120
H	0.0176247	1.5535109	1.7244220

$[\mathrm{Ni\,NTA\,(H_2O)_2}]^-$

C	0.5110899	1.1875097	-1.4444946
C	-1.7367804	0.8937460	-0.4728236
C	-0.5042033	-1.0839930	-1.2754595
O	1.6851026	3.2347823	-1.0311078
O	-3.1610734	1.7839049	1.2156565
O	-1.2376814	-3.2468208	-0.5507355
O	1.3465345	1.8686530	0.7227040
O	-1.2151034	0.8946573	1.8970995
C	1.2244366	2.1944521	-0.5157005
C	-2.0675974	1.2231793	0.9942179
C	-0.7489355	-2.1560172	-0.1899900
N	-0.4037310	0.2814528	-0.7179070
Ni	0.4678923	0.0288026	1.1507814
O	1.2731833	-0.1891247	3.1660550
H	-0.0080771	1.7272016	-2.2482254
H	1.3026846	0.5825718	-1.9048444
H	-2.5210563	0.2161737	-0.8345897
H	-1.8311126	1.8205048	-1.0532630
H	0.4540573	-1.3368166	-1.7468714
H	-1.2849671	-1.1527090	-2.0460326
H	1.1381225	-1.1026504	3.4714417
H	0.6953918	0.3440835	3.7395959
O	-0.3819816	-1.8732855	1.0110743
O	2.3336268	-0.8987373	0.3470927
H	3.0983542	-0.4042470	0.6870899
H	2.4350042	-1.7971537	0.7043865

$[\mathrm{Ni\,(H_2O)_6}]^{2+}$

Ni	-1.9210515	0.9836383	-0.0429388
O	-0.4439840	0.2181953	-1.2907074
H	0.4052722	0.6836074	-1.1893640
O	-3.3955044	1.7500555	1.2057954
H	-4.2441487	1.2832259	1.1057034
O	-1.5168079	-0.6186926	1.2186469
H	-0.9552658	-1.2911046	0.7934735
O	-2.3243096	2.5850560	-1.3052185
H	-1.5652708	3.0390703	-1.7100487
O	-3.4499999	-0.0196041	-1.0308042
H	-3.3110784	-0.9613037	-1.2311422
O	-0.3913137	1.9870969	0.9449054
H	-0.5321443	2.9282551	1.1464704
H	-0.6206787	0.2021080	-2.2470889
H	-3.2150769	1.7609258	2.1615867
H	-2.2740991	-1.1057270	1.5869342

H	-2.8484279	3.2835627	-0.8744556
H	-3.6878701	0.3961338	-1.8785986
H	-0.1515305	1.5712812	1.7921311

$[Cu\,NTA\,H_2O]^-$

C	0.0265587	1.2516992	-4.6275736
C	-2.2557288	0.4075393	-4.2105240
C	-0.4046418	-1.1794600	-4.6279581
O	2.3042212	1.9739062	-4.4410203
O	-3.8198349	1.9523929	-3.2451942
O	-0.6333480	-3.4784450	-3.9862128
O	1.4056748	0.8752749	-2.6925148
O	-2.0243238	1.3760067	-2.0196675
C	1.3693678	1.3725316	-3.8772917
C	-2.7511027	1.3373392	-3.0860087
C	-0.5819140	-2.3017040	-3.5867137
N	-0.8034556	0.1451942	-4.0998677
Cu	-0.4437910	0.0876997	-2.1284330
O	-0.1218814	0.0449927	-0.1324571
H	-0.5143272	2.1947671	-4.4730513
H	0.1907870	1.1319416	-5.7064225
H	-2.7894800	-0.5456859	-4.1006147
H	-2.5038977	0.8192920	-5.1976924
H	0.6637078	-1.1446279	-4.8774624
H	-0.9546920	-1.4125897	-5.5491694
H	-0.0805032	-0.8700100	0.1977200
H	-0.8677591	0.4515016	0.3434534
O	-0.6165118	-1.9361874	-2.3501667

$[Cu\,(H_2O)_6]^{2+}$

Cu	-1.9171905	0.9811935	-0.0428884
O	-0.5132542	0.2421176	-1.2766680
H	0.3420575	0.6867782	-1.1294085
O	-3.3199539	1.7227805	1.1909045
H	-4.1778577	1.2841998	1.0405585
O	-1.4458826	-0.7665614	1.4020073
H	-0.8987137	-1.4752016	1.0238711
O	-2.3969571	2.7305278	-1.4875008
H	-1.6902106	3.1805141	-1.9792504
O	-3.4110597	0.0819733	-1.0405559
H	-3.2781176	-0.8523668	-1.2814660
O	-0.4239048	1.8848544	0.9516712
H	-0.5569706	2.8212697	1.1843621
H	-0.6910718	0.3269309	-2.2305859
H	-3.1440308	1.6324949	2.1446733
H	-2.1597083	-1.2288601	1.8716374
H	-2.9260865	3.4484618	-1.1013881
H	-3.6046644	0.5554564	-1.8714473
H	-0.2297131	1.4192172	1.7867539

H_2O

O	-3.3006173	2.2577663	0.000000
H	-4.0301066	2.8983985	0.000000
H	-2.5046061	2.8136052	0.000000